

EFFICIENT QUANTUM CIRCUITS FOR PORT-BASED TELEPORTATION

DMITRY GRINKO¹, ADAM BURCHARDT¹, AND MARIS OZOLS^{1,2}

ABSTRACT. Port-based teleportation (PBT) is a variant of quantum teleportation that, unlike the canonical protocol by Bennett et al., does not require a correction operation on the teleported state. Since its introduction by Ishizaka and Hiroshima in 2008, no efficient implementation of PBT was known. We close this long-standing gap by building on our recent results on representations of partially transposed permutation matrix algebras and mixed quantum Schur transform. We describe efficient quantum circuits for probabilistic and deterministic PBT protocols on n ports of arbitrary local dimension, both for EPR and optimized resource states. We describe two constructions based on different encodings of the Gelfand–Tsetlin basis for n qudits: a standard encoding that achieves $\tilde{O}(n)$ time and $O(n \log(n))$ space complexity, and a Yamanouchi encoding that achieves $\tilde{O}(n^2)$ time and $O(\log(n))$ space complexity, both for constant local dimension and target error. We also describe efficient circuits for preparing the optimal resource states.

CONTENTS

1. Introduction	1
1.1. Background	1
1.2. Types of PBT protocols	2
1.3. Summary of our results	2
1.4. Related work	3
2. Preliminaries	3
2.1. Notation	3
2.2. Representation theory of the partially transposed permutation algebra	4
2.3. Mixed quantum Schur transform	5
2.4. PBT measurement and figures of merit	6
2.5. Optimal POVMs for port-based teleportation protocols	7
2.6. Naimark’s dilation and implementation of measurements	8
3. Efficient quantum algorithms for PBT in standard encoding	9
3.1. The standard PGM in the Gelfand–Tsetlin basis	9
3.2. Naimark’s dilation of the standard PGM	10
3.3. Quantum circuit for the standard PGM	12
3.4. Efficient quantum algorithms for generic PBT measurements	15
3.5. Exponentially improved lower bound for non-local quantum computation	16
4. Logarithmic space PBT via Yamanouchi encoding	16
5. Quantum circuits for optimized resource states	18
Acknowledgements	21
References	21

1. INTRODUCTION

1.1. **Background.** Quantum teleportation is a cornerstone of quantum information [Ben+93]. However, one potentially undesirable feature of the original teleportation protocol is that the receiving party needs to perform a correction operation on the received state. *Port-based teleportation* (PBT) gets around this limitation [IH08; IH09]. In PBT, Alice and Bob share an entangled resource state distributed among n quantum systems called *ports* on each side. To teleport an unknown quantum state, Alice measures it together with her share of the ports. The measurement outcome, which she communicates to Bob, indicates the port on Bob’s side to which the state has been teleported. Bob does not need to perform any correction operation but simply retrieve the state from the correct port. Each of the quantum systems involved has a fixed *local dimension* d .

¹INSTITUTE FOR LOGIC, LANGUAGE, AND COMPUTATION, UNIVERSITY OF AMSTERDAM AND QUSOFT, AMSTERDAM, THE NETHERLANDS

²KORTEWEG-DE VRIES INSTITUTE FOR MATHEMATICS AND INSTITUTE FOR THEORETICAL PHYSICS, UNIVERSITY OF AMSTERDAM, THE NETHERLANDS

E-mail addresses: dmitry.grinko@cwi.nl, adam.burchardt@cwi.nl, marozols@gmail.com.

Our current understanding of PBT protocols is very detailed thanks to a long sequence of works [IH08; IH09; BK11; Ish15; SSMH17; MSSH18; Led20; Chr+21]. In particular, [SSMH17; MSSH18] were the first to obtain exact formulas for the asymptotic performance of PBT. The resource requirements for PBT have been studied further in [SMK22; SS23]. The original PBT protocol has subsequently been extended to multi-port teleportation [SMKH22; KMSH21; MSK21] where several systems are teleported simultaneously.

A crucial feature of port-based teleportation is unitary equivariance [GO22], meaning that applying any unitary on Alice’s input state is equivalent to applying the same unitary to all of Bob’s ports. Due to unitary equivariance, PBT can be seen as a concrete example of an approximate universal programmable quantum processor [IH08]. The quantum no-programming theorem [NC97; GBW21; YRC20] implies that unitarily equivariant PBT protocols with a finite-dimensional resource state can only achieve approximate teleportation. Nevertheless, certain PBT protocols are asymptotically faithful in the limit of a large number of ports.

PBT has diverse applications in non-local quantum computation and quantum communication [BK11; Buh+16; May22] with applications to quantum position verification [ABSL22; ABMSL23], channel discrimination [PLLP19], channel simulation [PBP21], and holography in high-energy physics [May19; May22].

1.2. Types of PBT protocols. The two main types of PBT protocols considered are *probabilistic exact* (pPBT) and *deterministic inexact* (dPBT) [SSMH17; MSSH18; Led20]. “Probabilistic” refers to the fact that the protocol has some nonzero probability of failure, while “deterministic” highlights no possibility of failure, i.e., the average success probability of the protocol is $p_{\text{succ}} = 1$. “Exact” means that the protocol achieves perfect normalized entanglement fidelity $F/p_{\text{succ}} = 1$, while “inexact” means that $F/p_{\text{succ}} < 1$.¹ Besides pPBT and dPBT, one can also consider *probabilistic inexact* protocols that interpolate between pPBT and dPBT. One concrete example is minimal PBT (mPBT) which is a modified version of dPBT [SS23].

Two types of resource states for PBT are typically considered: n pairs of maximally entangled states and an arbitrary optimized state; we call these the *EPR resource state* and the *optimized resource state*, respectively. Depending on application, Alice’s measurement is chosen either to maximize the entanglement fidelity F (in dPBT) or the average success probability p_{succ} (in pPBT). While the optimized resource states are different for deterministic and probabilistic protocols, the optimal measurement for optimized states turns out to be the same in both cases. Table 1 summarizes the four main types of PBT protocols and their optimal fidelity and probability of success.

Resource state	Protocol type	
	Deterministic	Probabilistic
EPR	$F = 1 - O(1/n)$ $p_{\text{succ}} = 1$	$F/p_{\text{succ}} = 1$ $p_{\text{succ}} = 1 - O(1/\sqrt{n})$
Optimized	$F = 1 - O(1/n^2)$ $p_{\text{succ}} = 1$	$F/p_{\text{succ}} = 1$ $p_{\text{succ}} = 1 - O(1/n)$

TABLE 1. Summary of different flavours of PBT protocols. Rows correspond to EPR and optimized resource states while columns correspond to deterministic (dPBT) [SSMH17; MSSH18; Led20; Chr+21] and probabilistic (pPBT) [SSMH17; Chr+21] protocols. Two figures of merit are used: the average success probability p_{succ} and the entanglement fidelity F (normalized by the success probability p_{succ}) as functions of the number of ports n (we ignore the dependence on the local dimension d). Cell colors correspond to different optimal POVMs: is the standard PGM E defined in eq. (27) while is the POVM E^* defined in eqs. (33), (34), (37) and (38).

1.3. Summary of our results. While analytic expressions for the optimal measurement operators in PBT were known [SSMH17; MSSH18; Led20], efficient quantum circuits that implement them were not known until our work. Our main result provides explicit quantum circuits for implementing PBT and analyzes their complexity.

Theorem 1.1. *The measurements for all four types of PBT protocols (deterministic/probabilistic and with optimized/EPR resource state) can be implemented in two ways with the following time and space complexities:*

- (1) *standard encoding:* $nd^4 \text{polylog}(n, d, 1/\epsilon)$ time and $(n + d)d \log(n) \text{polylog}(d, 1/\epsilon)$ space,
- (2) *Yamanouchi encoding:* $n^2d^4 \text{polylog}(n, d, 1/\epsilon)$ time and $d^2 \log(n) \text{polylog}(d, 1/\epsilon)$ space,

¹For brevity, in the rest of this section we will drop the terms “exact” and “inexact” in these cases since deterministic PBT protocols with finite resources are always inexact, and exact protocols cannot be deterministic due to [NC97]. Of course, there is still a possibility of having probabilistic inexact protocols.

where n is the number of ports, d is the dimension of the teleported quantum state, and ϵ is the target error. In both cases the total gate complexity is the same: $n^2 d^4 \text{polylog}(n, d, 1/\epsilon)$.

The proof is explained in detail in the next sections. Our construction works also for a large class of generic PBT protocols (see Section 3.4 for more details). The setting of port-based teleportation is naturally suited for using the representation theory of the matrix algebra $\mathcal{A}_{n,1}^d$ of partially transposed permutations [GO22; GBO23]. It is also natural to work in the mixed Schur basis, which can be achieved by applying the mixed quantum Schur transform [GBO23; Ngu23].

1.4. Related work. The main idea of Naimark’s dilation behind the efficient construction of dPBT was initially presented in version 1 of our paper [GBO23]. This material is now presented in Section 3.4 with more details and expanded analysis. The constructions of all PBT protocols presented in the current paper can be seen as a straightforward generalization of this main idea presented in [GBO23].

Our initial result for deterministic PBT from [GBO23] was obtained independently and simultaneously with [FTH23], which solves the problem differently. A relevant independent construction of mixed quantum Schur transform was obtained in [Ngu23] together with our construction in [GBO23]. Moreover, a logarithmic space qubit Schur transforms described in [KS18; WS23] inspired our Yamanouchi encoding construction presented in Section 4.

Finally, in the course of writing this manuscript, we became aware of the independent work [WHS23] which tackles specifically the qubit case for all PBT protocols. In contrast to [WHS23], our independent result solves the problem for dPBT and pPBT protocols for arbitrary local dimensions in full generality, achieving better time complexities. On the technical side, both results [FTH23; WHS23] construct their PBT protocols by using general techniques of block encodings and oblivious amplitude amplification, while our construction requires neither technique and is based on the phase estimation primitive. This leads to more practical circuits and more appealing theoretical analysis. These features of our constructions are enabled by proper use of the representation theory of partially transposed permutation matrix algebras via the Gelfand–Tsetlin basis which we developed in [GBO23], see also [GO22].

2. PRELIMINARIES

2.1. Notation. Let $n \geq 0$ be an integer. We write $\lambda \vdash n$ to mean that λ is a *partition* of n , i.e., $\lambda = (\lambda_1, \dots, \lambda_d)$ for some d where $\lambda_1 + \dots + \lambda_d = n$ and $\lambda_1 \geq \dots \geq \lambda_d \geq 0$. The *size* of partition λ is $|\lambda| = n$. We say that λ has *length* $\ell(\lambda) = k$ if $\lambda_k > 0$ and $\lambda_{k+1} = 0$. We use the notation $\lambda \vdash_d n$ to indicate that $\lambda \vdash n$ and $\ell(\lambda) \leq d$. The *Young diagram* of partition λ is a collection of n *cells* arranged in $\ell(\lambda)$ rows, with λ_i of them in the i -th row. For example,

$$\begin{array}{|c|c|c|} \hline & & \\ \hline & & \\ \hline & & \\ \hline \end{array} \quad (1)$$

is the Young diagram of partition $\lambda = (3, 2)$. We will use these two notions interchangeably.

Any cell $u \in \lambda$ can be specified by its row and column coordinates i and j . The *content* of cell $u = (i, j)$ is

$$\text{cont}(u) := j - i. \quad (2)$$

For example, the cells of the Young diagram $(3, 2)$ have the following content:

$$\begin{array}{|c|c|c|} \hline 0 & 1 & 2 \\ \hline -1 & 0 & \\ \hline \end{array}. \quad (3)$$

Note that content is constant on diagonals of λ and increases by one when going right or up, and decreases by one when going left or down.

A cell $u \in \lambda$ is called *removable* if the diagram $\lambda \setminus u$ obtained by removing u from λ is a valid Young diagram. Similarly, a cell $u \notin \lambda$ is called *addable* if the diagram $\lambda \cup u$ obtained by adding u to λ is a valid Young diagram. We will denote the sets of all removable and addable cells of λ by $\text{RC}(\lambda)$ and $\text{AC}(\lambda)$, respectively. Furthermore, $\text{AC}_d(\lambda) \subseteq \text{AC}(\lambda)$ denotes the subset of addable cells a of λ such that $\lambda \cup a$ has at most d rows:

$$\text{AC}_d(\lambda) := \{a \in \text{AC}(\lambda) \mid \ell(\lambda \cup a) \leq d\}. \quad (4)$$

For example, the Young diagram $\lambda = (5, 3, 3)$ (shown in gray) has two removable cells: $r_1 = (1, 5)$, $r_2 = (3, 3)$, and three addable cells: $a_1 = (1, 6)$, $a_2 = (2, 4)$, $a_3 = (4, 1)$:

$$\begin{array}{|c|c|c|c|c|c|} \hline & & & & r_1 & a_1 \\ \hline & & & & a_2 & \\ \hline & & r_2 & & & \\ \hline a_3 & & & & & \\ \hline \end{array}. \quad (5)$$

2.2. Representation theory of the partially transposed permutation algebra. The setting of PBT is naturally suited for certain tools from representation theory, such as mixed Schur–Weyl duality for the matrix algebra of partially transposed permutations [GBO23]. Here we present a short introduction to these topics and refer the reader to [GBO23] for more details.

The matrix algebra $\mathcal{A}_{n,1}^d$ of *partially transposed permutations* acts on $n + 1$ qudits, each of local dimension d . Its generators $\sigma_1, \dots, \sigma_n$ act on $(\mathbb{C}^d)^{\otimes n+1}$ in the following way: for all $x_1, \dots, x_{n+1} \in [d] := \{1, \dots, d\}$,

$$\sigma_i |x_1, \dots, x_{n+1}\rangle := \begin{cases} |x_1, \dots, x_{i+1}, x_i, \dots, x_{n+1}\rangle, & i \neq n, \\ |x_1, \dots, x_{n-1}\rangle \otimes \delta_{x_n, x_{n+1}} \sum_{k=1}^d |k, k\rangle, & i = n. \end{cases} \quad (6)$$

In other words, σ_i with $i < n$ are *transpositions* that exchange qudits i and $i + 1$, while σ_n is a *contraction* that projects the last two qudits on the un-normalized maximally entangled state. The irreducible representations or *irreps* of $\mathcal{A}_{n,1}^d$ are labelled by the following pairs of Young diagrams of two types:

$$\widehat{\mathcal{A}}_{n,1}^d := \left\{ (\lambda, \emptyset) \mid \lambda \vdash n - 1, \ell(\lambda) \leq d \right\} \sqcup \left\{ (\mu, \square) \mid \mu \vdash n, \ell(\mu) \leq d - 1 \right\}, \quad (7)$$

where \emptyset denotes the empty diagram and $\square = (1)$. More generally, the irreducible representations of $\mathcal{A}_{n,m}^d$ for arbitrary $n, m \geq 0$ are labelled by pairs of partitions $\Lambda = (\lambda, \lambda')$ such that $\ell(\lambda) + \ell(\lambda') \leq d$ and $\lambda \vdash n - k$ and $\lambda' \vdash m - k$ for some $0 \leq k \leq \min(n, m)$ [GBO23] (in our case $m = 1$ and $k = 0, 1$). We slightly abuse notation by not including d as part of Λ since d is assumed to be fixed throughout. However, knowing d is necessary to unambiguously convert Λ into a *staircase* of length d , which is another convenient way of labelling the irreps of $\mathcal{A}_{n,m}^d$ [Ste87; GBO23].

To describe the representation theory of $\mathcal{A}_{n,1}^d$, we employ the so-called Okounkov–Vershik approach. A central notion in this approach is the *Bratteli diagram* \mathcal{B} for the sequence of algebras $\mathcal{A}_{0,0}^d \hookrightarrow \mathcal{A}_{1,0}^d \hookrightarrow \dots \hookrightarrow \mathcal{A}_{n,0}^d \hookrightarrow \mathcal{A}_{n,1}^d$, which is a directed acyclic simple graph obtained as follows. The vertices of \mathcal{B} are divided into $n + 2$ *levels* denoted by $i = 0, \dots, n + 1$. These levels correspond to sets of irreducible representations $\widehat{\mathcal{A}}_{0,0}^d, \widehat{\mathcal{A}}_{1,0}^d, \dots, \widehat{\mathcal{A}}_{n,1}^d$ of the corresponding algebras $\mathcal{A}_{0,0}^d, \mathcal{A}_{1,0}^d, \dots, \mathcal{A}_{n,1}^d$. The vertices at level $i \in \{0, \dots, n\}$ are labelled by Young diagrams $\lambda \vdash i$ with $\ell(\lambda) \leq d$, while the vertices at the last level $n + 1$ are labelled by pairs of Young diagrams Λ corresponding to the irreps $\widehat{\mathcal{A}}_{n,1}^d$, see eq. (7). When $i \in \{0, \dots, n\}$, the vertices $\mu \vdash i - 1$ and $\lambda \vdash i$ are connected, denoted as $\mu \rightarrow \lambda$, if λ can be obtained from μ by adding a cell, i.e., $\lambda = \mu \cup a$ for some $a \in \text{AC}_d(\mu)$. Furthermore, a vertex $\mu \vdash n$ at level n is connected to Λ at level $n + 1$ iff $\Lambda = (\mu, \square)$ for $\ell(\mu) \leq d - 1$ or $\Lambda = (\lambda, \emptyset)$ if μ can be obtained by adding a cell to λ , i.e., $\mu = \lambda \cup a$ for some $a \in \text{AC}_d(\lambda)$. The Bratteli diagram \mathcal{B} consists of all vertices from all levels and the directed edges between them (see Fig. 1 for an example). We denote the only vertex at level 0 by \emptyset and call it *root*, while the vertices at the last level of \mathcal{B} we call *leaves* (they correspond bijectively to the irreps $\widehat{\mathcal{A}}_{n,1}^d$). For any leaf $\Lambda \in \widehat{\mathcal{A}}_{n,1}^d$, we denote by

$$\text{Paths}(\Lambda, \mathcal{B}) := \left\{ (T^0, T^1, \dots, T^n, T^{n+1}) \mid T^k \vdash k \text{ for } k \leq n, T^{i-1} \rightarrow T^i \text{ for } i \in [n+1] \text{ and } T^{n+1} = \Lambda \right\} \quad (8)$$

the set of all paths in \mathcal{B} starting at the root $T^0 = \emptyset$ and terminating at Λ . If $i \in [n]$ is an intermediate position on a path T , the diagram T^i is obtained from T^{i-1} by adding some addable cell $a \in \text{AC}_d(T^{i-1})$, hence $T^i \setminus T^{i-1}$ consists of a single cell. For any path $T = (T^0, \dots, T^{n+1}) \in \text{Paths}(\Lambda, \mathcal{B})$ and $i \in [n]$ we define the *content* of i in T as

$$\text{cont}_i(T) := \text{cont}(T^i \setminus T^{i-1}) \quad (9)$$

and the *axial distance* between i and $i + 1$ in T as

$$r_i(T) = \text{cont}_{i+1}(T) - \text{cont}_i(T). \quad (10)$$

Similar to eq. (8), for any intermediate vertex $\lambda \vdash k$ at level $k \leq n$ in \mathcal{B} , we use $\text{Paths}_k(\lambda, \mathcal{B})$ to denote the set of all paths in \mathcal{B} terminating at λ . Furthermore, we denote by $\text{Paths}(\mathcal{B})$ the set of all paths in \mathcal{B} , i.e., $\text{Paths}(\mathcal{B}) := \bigsqcup_{\Lambda \in \widehat{\mathcal{A}}_{n,1}^d} \text{Paths}(\Lambda, \mathcal{B})$.

The Bratteli diagram \mathcal{B} plays an important role in the representation theory of $\mathcal{A}_{n,1}^d$ [GO22; GBO23]. Recall that the vertices on the last level of \mathcal{B} correspond to irreducible representations $\widehat{\mathcal{A}}_{n,1}^d$ of $\mathcal{A}_{n,1}^d$. For a given $\Lambda \in \widehat{\mathcal{A}}_{n,1}^d$, the corresponding irrep ψ_Λ has a convenient explicit description in the so-called *Gelfand–Tsetlin basis* $\{|T\rangle \mid T \in \text{Paths}(\Lambda, \mathcal{B})\}$ which is spanned by all paths from \emptyset to Λ in \mathcal{B} . Recall from eq. (6) that $\mathcal{A}_{n,1}^d$ is generated by $n - 1$ transpositions $\sigma_1, \dots, \sigma_{n-1}$ and one contraction σ_n . For any irrep $\Lambda \in \widehat{\mathcal{A}}_{n,1}^d$, a transposition σ_i acts on a given path $T \in \text{Paths}(\Lambda, \mathcal{B})$ as follows:

$$\psi_\Lambda(\sigma_i) |T\rangle = \frac{1}{r_i(T)} |T\rangle + \sqrt{1 - \frac{1}{r_i(T)^2}} |\sigma_i T\rangle \quad \text{for } i \neq n, \quad (11)$$

where $\sigma_i T$ denotes the path T with vertex T^i at level i replaced by $T^{i-1} \cup (T^{i+1} \setminus T^i)$. Equation (11) coincides with the well-known Young–Yamanouchi basis for the symmetric group S_n . The remaining generator σ_n acts

trivially in irreps $\Lambda = (\mu, \square)$:

$$\psi_{(\mu, \square)}(\sigma_n) |T\rangle = 0. \quad (12)$$

To describe the action of σ_n in the remaining irreps $\Lambda = (\lambda, \emptyset)$, notice that any path $T \in \text{Paths}((\lambda, \emptyset), \mathcal{B})$ is of the form $T = S \circ (\lambda \cup a) \circ (\lambda, \emptyset)$ for some prefix $S \in \text{Paths}_{n-1}(\lambda, \mathcal{B})$, partition $\lambda \vdash n-1$, and addable cell $a \in \text{AC}_d(\lambda)$, where \circ extends the path by appending new vertices. The generator σ_n acts on such path in the following way (see [GBO23, Theorem 3.2]):

$$\psi_{(\lambda, \emptyset)}(\sigma_n) |S \circ (\lambda \cup a) \circ (\lambda, \emptyset)\rangle = \sum_{a' \in \text{AC}_d(\lambda)} \frac{\sqrt{m_{\lambda \cup a} m_{\lambda \cup a'}}}{m_\lambda} |S \circ (\lambda \cup a') \circ (\lambda, \emptyset)\rangle, \quad (13)$$

where m_λ denotes the dimension of the λ -irrep of the unitary group U_d . According to the well-known *Weyl dimension* [Lou08, eq. (11.46)] and *hook-content* formulas, m_λ can be computed for a given Young diagram λ as

$$m_\lambda = \prod_{1 \leq i < j \leq d} \frac{\lambda_i - \lambda_j + j - i}{j - i} = \prod_{c \in \lambda} \frac{d + \text{cont}(c)}{h_\lambda(c)}, \quad (14)$$

where c ranges over all cells in λ and $h_\lambda(c)$ is the *hook length* of c in λ . Weyl dimension formula also works for a general staircase Λ :

$$m_\Lambda = \prod_{1 \leq i < j \leq d} \frac{\Lambda_i - \Lambda_j + j - i}{j - i}. \quad (15)$$

2.3. Mixed quantum Schur transform. A generalization of Schur–Weyl duality known as *mixed Schur–Weyl duality* [GO22; GBO23]. A variant of mixed Schur–Weyl duality partitions the space $(\mathbb{C}^d)^{\otimes n+1}$ into subspaces that are invariant under the natural $U^{\otimes n} \otimes \bar{U}$ action of $U \in U_d$ and the action (6) of the matrix algebra $\mathcal{A}_{n,1}^d$. Moreover, there exists a unitary basis change $U_{\text{Sch}}(n, 1) \in U_{d^{n+1}}$ known as *mixed quantum Schur transform* [GBO23; Ngu23] that maps the computational basis $\{|x\rangle \mid x \in [d]^{n+1}\}$ of $(\mathbb{C}^d)^{\otimes n+1}$ to a new basis composed of irreducible representations \mathcal{W}_Λ and \mathcal{H}_Λ of the aforementioned actions of U_d and $\mathcal{A}_{n,1}^d$, respectively:

$$U_{\text{Sch}}(n, 1): (\mathbb{C}^d)^{\otimes n+1} \rightarrow \bigoplus_{\Lambda \in \widehat{\mathcal{A}}_{n,1}^d} \mathcal{H}_\Lambda \otimes \mathcal{W}_\Lambda \quad \text{where} \quad \mathcal{H}_\Lambda := \mathbb{C}^{\text{Paths}(\Lambda, \mathcal{B})} \quad \text{and} \quad \mathcal{W}_\Lambda := \mathbb{C}^{\text{GT}(\Lambda)}. \quad (16)$$

Here the direct sum ranges over all irreducible representations Λ of $\mathcal{A}_{n,1}^d$, see eq. (7), and $\text{GT}(\Lambda)$ denotes the set of, so-called, Gelfand–Tsetlin patterns of shape Λ (they index a natural basis for the Λ -irrep of the unitary group U_d , see [GBO23] for more details). We will denote the dimensions of \mathcal{H}_Λ and \mathcal{W}_Λ by

$$d_\Lambda := \dim \mathcal{H}_\Lambda = |\text{Paths}(\Lambda, \mathcal{B})|, \quad (17)$$

$$m_\Lambda := \dim \mathcal{W}_\Lambda = |\text{GT}(\Lambda)|. \quad (18)$$

Note that both irrep dimensions implicitly depend on the local dimension d which is implicit in Λ . Moreover, for any path $T \in \text{Paths}(\Lambda, \mathcal{B})$ and for any level k but the last, the dimension d_{T^k} coincides with the dimension of the corresponding T^k -irrep of the symmetric group S_k . As Schur transform (16) is a basis transformation, the non-trivial combinatorial identity $d^{n+1} = \sum_{\Lambda \in \widehat{\mathcal{A}}_{n,1}^d} d_\Lambda m_\Lambda$ holds true. Any element $\sigma \in \mathcal{A}_{n,1}^d$, such as the generators σ_i from eq. (6), transform by Schur transform as follows:

$$U_{\text{Sch}}(n, 1) \sigma U_{\text{Sch}}^\dagger(n, 1) = \bigoplus_{\Lambda \in \widehat{\mathcal{A}}_{n,1}^d} \psi_\Lambda(\sigma) \otimes I_{m_\Lambda}, \quad (19)$$

where ψ_Λ denotes the corresponding d_Λ -dimensional irrep of $\mathcal{A}_{n,1}^d$ defined by eqs. (11) to (13).

The mixed quantum Schur transform (16) is a basis change that maps the computational basis into the mixed Schur basis and hence is a unitary operator. The mixed Schur basis is labelled by pairs of vectors $|T, M\rangle$, where M is a Gelfand–Tsetlin pattern and $T = (T^1, \dots, T^{n+1}) \in \text{Paths}(\mathcal{B})$ is a path in the Bratteli diagram \mathcal{B} . Notice that the set of all paths in \mathcal{B} is not a Cartesian product of allowed vertices in each level, i.e., $\text{Paths}(\mathcal{B}) \neq \widehat{\mathcal{A}}_{0,0}^d \times \dots \times \widehat{\mathcal{A}}_{n,1}^d$, as consecutive vertices in a valid path $T \in \text{Paths}(\mathcal{B})$ must differ only by one cell. However, the set of all paths in \mathcal{B} is naturally embedded in the set $\widehat{\mathcal{A}}_{0,0}^d \times \dots \times \widehat{\mathcal{A}}_{n,1}^d$. We call the mixed quantum Schur transform based on this embedding a *mixed Schur isometry*

$$U_{\text{Sch}}(n, 1): (\mathbb{C}^d)^{\otimes n+1} \rightarrow \underbrace{\mathbb{C}^{\widehat{\mathcal{A}}_{0,0}^d} \otimes \dots \otimes \mathbb{C}^{\widehat{\mathcal{A}}_{n,1}^d}}_T \otimes \underbrace{\mathbb{C}^{\text{GT}((n,1),d)}}_{M_{[d-1]}}, \quad (20)$$

to distinguish it from the unitary transformation (16), where $M_{[d-1]}$ denotes the Gelfand–Tsetlin pattern M without the top d -th row (the subscript means that we keep only the bottom $d-1$ rows of M). In [GBO23], we described a quantum circuit implementing the mixed Schur isometry, which for any computational basis vector outputs the corresponding superposition of paths $T \in \text{Paths}(\mathcal{B})$ and Gelfand–Tsetlin patterns without top row $M_{[d-1]} \in \text{GT}((n, 1), d)$, where $\text{GT}((n, 1), d) := \{M_{[d-1]} \mid M \in \bigsqcup_{\Lambda \in \widehat{\mathcal{A}}_{n,1}^d} \text{GT}(\Lambda)\}$. The complexity of

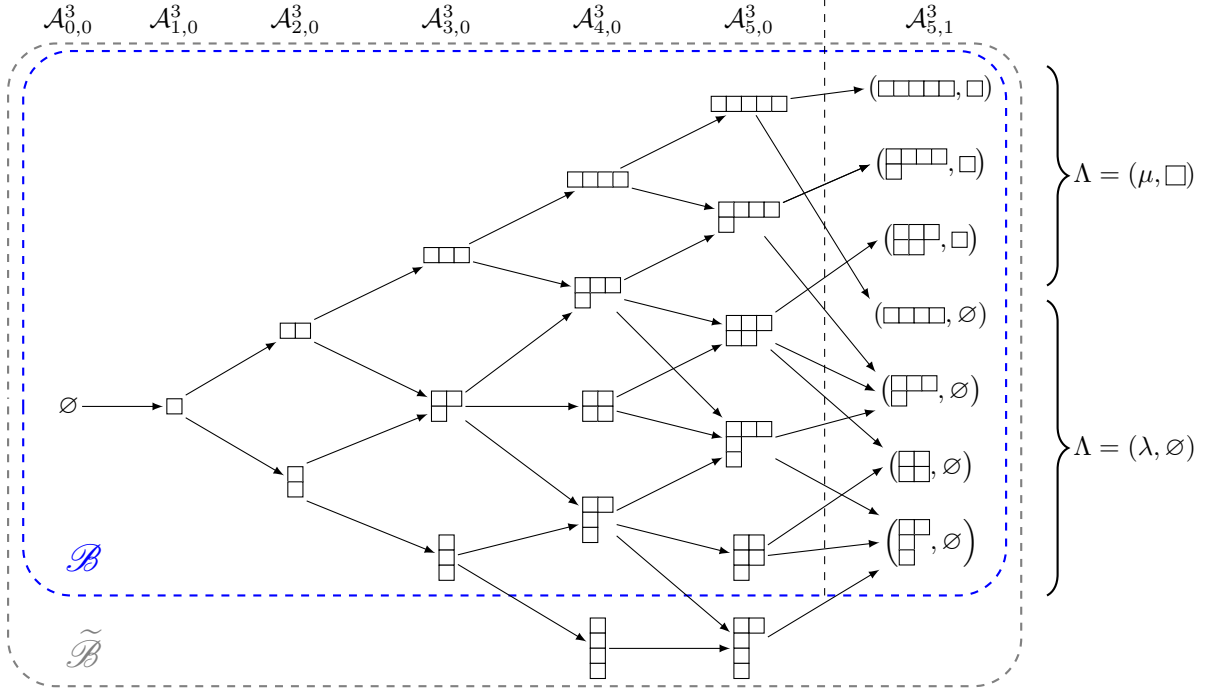


FIGURE 1. The Bratteli diagram \mathcal{B} and the extended Bratteli diagram $\tilde{\mathcal{B}}$ associated with the algebra $\mathcal{A}_{5,1}^3$. Vertices in the last column correspond to the set $\hat{\mathcal{A}}_{5,1}^3$ of irreducible representations of $\mathcal{A}_{5,1}^3$. A vector space corresponding to an irrep $\Lambda \in \hat{\mathcal{A}}_{5,1}^3$ is spanned by $\text{Paths}(\Lambda, \mathcal{B})$ the set of all paths terminating at Λ , eqs. (11) to (13) describe the action of the generators σ_i of the algebra $\mathcal{A}_{5,1}^3$ in corresponding irrep. Irreps $\Lambda \in \hat{\mathcal{A}}_{5,1}^3$ are of two different types: either $\Lambda = (\lambda, \emptyset)$, or $\Lambda = (\mu, \square)$. POVMs implementing optimal measurements for PBT protocols are supported only on irreps corresponding to $\Lambda = (\lambda, \emptyset)$. The extension of \mathcal{B} to $\tilde{\mathcal{B}}$ allows the implementation of optimal POVMs as PVMs, see Section 3.2.

implementing the mixed quantum Schur transform is $\tilde{O}(nd^4)$ [Ngu23; GBO23]. Notice from eq. (20) that a path $T \in \text{Paths}(\mathcal{B})$ is stored as a tensor product state

$$|T\rangle = |T^2\rangle \otimes \dots \otimes |T^{n+1}\rangle, \quad (21)$$

where we have suppressed the registers $|T^0\rangle$ and $|T^1\rangle$ since they are one-dimensional ($T^0 = \emptyset$ and $T^1 = \square$ for any path T). T^{n+1} represents the irrep label, which we usually refer to as $T^{n+1} = \Lambda$. We call eq. (21) the *standard encoding* of $|T\rangle$.

We will also consider another more space-efficient isometry implementing the mixed quantum Schur transform. Notice that for a given path $T = (T^0, \dots, T^{n+1}) \in \text{Paths}(\Lambda, \mathcal{B})$, the vertex T^i is uniquely determined by the previous vertex T^{i-1} and the row number y_i of the added (or removed) box $T^i \setminus T^{i-1}$. The sequence (y_1, \dots, y_{n+1}) is called the *Yamanouchi word* of path T . Since $y_i \in [d]$ for each i , encoding a path T as a sequence of y_i instead of T^i is more space-efficient. Indeed, each y_i can be stored directly in the i -th input qudit without requiring additional memory, while storing each T^i takes $O(d \log n)$ qubits and thus $O(nd \log n)$ auxiliary qubits for T in total. We call this more efficient encoding of the mixed Schur transform the *Yamanouchi encoding*:

$$U_{\text{Sch}}(n, 1): (\mathbb{C}^d)^{n+1} \rightarrow \underbrace{\mathbb{C}^d \otimes \dots \otimes \mathbb{C}^d}_{(y_1, \dots, y_{n+1})} \otimes \underbrace{\mathbb{C}^{\hat{\mathcal{A}}_{n,1}^d}}_{\Lambda} \otimes \underbrace{\mathbb{C}^{\text{GT}((n,1),d)}}_{M_{[d-1]}}. \quad (22)$$

More specifically, we store a path $T \in \text{Paths}(\mathcal{B})$ as the following tensor product state:

$$|T\rangle = |y_2\rangle \otimes \dots \otimes |y_n\rangle \otimes |y_{n+1}\rangle \otimes |\Lambda\rangle, \quad (23)$$

where the first register $|y_1\rangle$ is suppressed since it is one-dimensional ($y_1 = 1$ for any path). While the Yamanouchi encoding is more space-efficient, it makes certain operations less time-efficient. For example, to recover the i -th vertex T^i of a path T , one needs to perform a certain computation on y_1, \dots, y_i stored in the first i registers of $|T\rangle$, as opposed to directly looking up the i -th register $|T^i\rangle$ in the standard encoding (21).

2.4. PBT measurement and figures of merit. In this section, we briefly describe the general setting of PBT and the relevant figures of merit. In a PBT protocol two parties, Alice and Bob, share a resource state distributed among n quantum systems called ports, each of local dimension d . We denote Alice's ports by

A_1, \dots, A_n and Bob's ports by B_1, \dots, B_n . Alice has an additional $(n+1)$ -th register \bar{A} on her side that contains an unknown input state $|\psi\rangle_{\bar{A}} \in \mathbb{C}^d$ that she must teleport to Bob.

The main ingredient of every PBT protocol is a measurement that is performed by Alice on all her registers A_1, \dots, A_n, \bar{A} . The rest of the protocol consists of Alice transmitting the measurement outcome to Bob who uses it to locate the teleported state on one of his ports. The most general measurement in quantum mechanics is known as *positive operator-valued measure* (POVM), which is described mathematically as follows.

Definition 2.1. A positive operator-valued measure (POVM) is a set $E := \{E_k\}_{k=1}^n$ of positive semi-definite matrices $E_k \geq 0$ that sum to the identity matrix: $\sum_{k=1}^n E_k = I$.

In dPBT, Alice's measurement has n outcomes and the outcome $k \in [n]$ indicates the port where Bob should find the teleported state $|\psi\rangle$. Probabilistic protocols, such as mPBT and pPBT, have an additional outcome $k = 0$ corresponding to the failure of the teleportation task.

We can describe a general PBT protocol in terms of a quantum channel \mathcal{N} :

$$\mathcal{N}_{\bar{A} \rightarrow \bar{B}}(\rho) := \sum_{k=1}^n \text{Tr}_{A^n \bar{A} B'_k} \left[\left((\sqrt{E_k})_{A^n \bar{A}} \otimes I_{B^n} \right) (\Psi_{A^n B^n} \otimes \rho_{\bar{A}}) \left(\sqrt{E_k}_{A^n \bar{A}} \otimes I_{B^n} \right) \right], \quad (24)$$

where $A^n := A_1 \dots A_n$ and $B^n := B_1 \dots B_n$ denote Alice's and Bob's ports, $B'_k := B^n \setminus B_k$ denotes all of Bob's ports but the k -th, $\Psi_{A^n B^n}$ is the resource state shared between Alice and Bob, $\rho_{\bar{A}}$ is the state to be teleported, and E_k are Alice's POVM operators. Note that the sum in eq. (24) omits the value $k = 0$, hence \mathcal{N} is trace-decreasing if Alice's POVM contains a failure operator $E_0 \neq 0$.

The following two figures of merit are commonly used for characterizing the performance of PBT. The *entanglement fidelity* of the protocol is given by

$$F := \text{Tr} \left[\Phi_{BR}^+ (\mathcal{N}_{\bar{A} \rightarrow \bar{B}} \otimes I_R) [\Phi_{AR}^+] \right] \quad (25)$$

where Φ_{AR}^+ denotes the two-qudit maximally entangled state between \bar{A} and a reference system R . The *average success probability* is given by

$$p_{\text{succ}} := \text{Tr} [\mathcal{N}_{\bar{A} \rightarrow \bar{B}}(I/d)], \quad (26)$$

which can be less than 1 since in general \mathcal{N} is trace-decreasing.

2.5. Optimal POVMs for port-based teleportation protocols. Let us now describe the optimal measurement for PBT, both in the standard and Schur basis. Recall that a special type of POVM called *pretty good measurement* (PGM) [HW94] is optimal for dPBT for both types of resource states, i.e., optimized and EPR [SSMH17; MSSH18; Led20]. Moreover, essentially the same measurement is also used in mPBT for both types of resource states [SS23]. We denote this POVM by $E = \{E_k\}_{k=0}^n$ and call it the *standard PGM*² for PBT:

$$E_k := \rho^{-1/2} \rho_k \rho^{-1/2} \text{ for every } k \in [n], \quad \rho := \sum_{k=1}^n \rho_k, \quad \rho_k := \pi^k \sigma_n \pi^{-k}, \quad E_0 := I - \sum_{k=1}^n E_k, \quad (27)$$

where ρ^{-1} is the generalized inverse of ρ ,

$$\pi := \sigma_1 \sigma_2 \dots \sigma_{n-2} \sigma_{n-1} \in \mathcal{A}_{n,1}^d \quad (28)$$

is the cyclic shift permutation $(1 \ 2 \ \dots \ n)$ on the first n systems, and $\sigma_n \in \mathcal{A}_{n,1}^d$ is the contraction between systems n and $n+1$ (it corresponds to the un-normalized projection onto the maximally entangled state between them). Since ρ commutes with $\mathcal{A}_{n,0}^d$ and thus with π , the POVM elements E_k for $k \in [n]$ can be written as

$$E_k = \pi^k E_n \pi^{-k} \quad \text{where} \quad E_n = \rho^{-1/2} \sigma_n \rho^{-1/2}, \quad (29)$$

hence the standard PGM is group-covariant [DJR04] with respect to the cyclic group on n elements.

The key to finding an efficient implementation of the measurement (27) will be expressing the operators E_k in the Schur basis (19). This requires deriving an explicit formula for $\psi_{\Lambda}(E_k)$ for any irrep $\Lambda \in \widehat{\mathcal{A}}_{n,1}^d$, which we will do in Section 3.1. For now, let us make some simple observations regarding $\psi_{\Lambda}(E_k)$.

Since ρ coincides with the shifted *Jucys–Murphy element* $d - J_{n+1}$ of $\mathcal{A}_{n,1}^d$, its spectrum can be easily computed, see [GBO23]. More concretely, ρ is nonzero and diagonal in the Gelfand–Tsetlin basis of each irrep $(\lambda, \varnothing) \in \widehat{\mathcal{A}}_{n,1}^d$:

$$\psi_{(\lambda, \varnothing)}(\rho) = \sum_{a \in \text{AC}_d(\lambda)} (d + \text{cont}(a)) \sum_{S \in \text{Paths}_{n-1}(\lambda, \varnothing)} |S \circ (\lambda \cup a) \circ (\lambda, \varnothing)\rangle \langle S \circ (\lambda \cup a) \circ (\lambda, \varnothing)|, \quad (30)$$

²Note that in the case of dPBT there is no $k = 0$ outcome since E_0 is distributed among the other operators (intuitively, upon obtaining outcome 0 Alice would send a uniformly random number $k \in [n]$ to Bob). Thus there are effectively only n outcomes. In the case of mPBT and optimized pPBT, Alice aborts the protocol upon measuring $k = 0$.

and $\psi_{(\mu, \square)}(\rho) = 0$ for every $(\mu, \square) \in \widehat{\mathcal{A}}_{n,1}^d$. In particular, $E_0 E_k = 0$ for every $k \in [n]$ or, more precisely, we have for every $k \in [n]$:

$$\psi_{(\mu, \square)}(E_k) = 0 \text{ for every } (\mu, \square) \in \widehat{\mathcal{A}}_{n,1}^d, \quad (31)$$

$$\psi_{(\lambda, \emptyset)}(E_0) = 0 \text{ for every } (\lambda, \emptyset) \in \widehat{\mathcal{A}}_{n,1}^d. \quad (32)$$

The optimal pPBT measurement for optimized state turns out to be equal to the standard PGM (27).³ In contrast, for pPBT with EPR resource state the optimal measurement is not the standard PGM. However, it is still closely related to the measurement E defined in eq. (27). Thanks to [Chr+21, Propositions 1.7 and 3.4], we can assume without loss of generality that the optimal measurement $E^* = \{E_k^*\}_{k=0}^n$ for a *generic PBT protocol* is given in the Gelfand–Tsetlin basis as

$$\psi_{(\lambda, \emptyset)}(E_k^*) := \sqrt{\psi_{(\lambda, \emptyset)}(G)} \psi_{(\lambda, \emptyset)}(E_k) \sqrt{\psi_{(\lambda, \emptyset)}(G)}, \quad (33)$$

$$\psi_{(\mu, \square)}\left(\sum_{k=1}^n E_k^*\right) := \psi_{(\mu, \square)}(G) \quad (34)$$

for some choice of $G \in \mathcal{A}_{n,1}^d$ such that G commutes with $\mathcal{A}_{n,0}^d$ and $I \succeq \psi_{\Lambda}(G) \succeq 0$ for every $\Lambda \in \widehat{\mathcal{A}}_{n,1}^d$. Equations (33) and (34) implies that

$$\psi_{(\lambda, \emptyset)}(E_0^*) = I - \psi_{(\lambda, \emptyset)}(G), \quad (35)$$

$$\psi_{(\mu, \square)}(E_0^*) = I - \psi_{(\mu, \square)}(G). \quad (36)$$

The actual value of $\psi_{(\mu, \square)}(E_k^*)$, $k \in [n]$ is not important since it does not affect the entanglement fidelity.

According to [SSMH17], the optimal POVM for pPBT with EPR resource state corresponds to G defined as

$$\psi_{\Lambda}(G) := \begin{cases} 0 & \text{if } \Lambda = (\mu, \square) \text{ where } \mu \vdash n, \\ \frac{\psi_{\Lambda}(\rho)}{d + \lambda_1} & \text{if } \Lambda = (\lambda, \emptyset) \text{ where } \lambda \vdash n - 1, \end{cases} \quad (37)$$

where $\psi_{\Lambda}(\rho)$ is given in eq. (30). The matrix $\psi_{(\lambda, \emptyset)}(G)$ is diagonal for every Λ and its diagonal entries $G_{\lambda,a}$ can be written for every $\lambda \vdash_d n - 1$ and $a \in \text{AC}_d(\lambda)$ as

$$G_{\lambda,a} := \frac{d + \text{cont}(a)}{d + \lambda_1}. \quad (38)$$

Note that λ_1 is the highest possible content among $a \in \text{AC}_d(\lambda)$, so $I \succeq \psi_{(\lambda, \emptyset)}(G) \succeq 0$. We provide a summary of the mentioned PBT protocols in Table 1, which is adapted from [SS23].

2.6. Naimark’s dilation and implementation of measurements. In this section, we state some facts about projection-valued measures, which we will need in the later sections to work with Naimark’s dilations of certain POVMs. First, recall that

Definition 2.2. $\Pi := \{\Pi_i\}_{i=1}^n$ is a projection-valued measure (PVM) on a given Hilbert space \mathcal{H} if $\sum_{i=1}^n \Pi_i = I_{\mathcal{H}}$ and Π_i is an orthogonal projection, i.e. $\Pi_i^2 = \Pi_i = \Pi_i^{\dagger} \succeq 0$, for every $i \in [n]$.

Remark 2.3. If $\{\Pi_i\}_{i=1}^n$ is a PVM then for every pair $i, j \in [n]$, $i \neq j$ the projectors Π_i and Π_j are mutually orthogonal, i.e. $\Pi_i \Pi_j = \delta_{i,j} \Pi_i$. Indeed, take a vector $|v\rangle \in \text{im}(\Pi_i) \subseteq \mathcal{H}$, and since $\sum_j \Pi_j = I_{\mathcal{H}}$ we have $1 + \sum_{j \neq i} \langle v | \Pi_j | v \rangle = 1$. Therefore, since each Π_j is positive semidefinite it must be $\langle v | \Pi_j | v \rangle = 0$ for every $j \neq i$, which implies $\Pi_i \Pi_j = \delta_{i,j} \Pi_i$. The converse is also true: if every pair of operators in a given POVM are mutually orthogonal then this POVM is a PVM.

Now assume that for a certain POVM with $n + 1$ outcomes $k \in \{0, 1, \dots, n\}$ we managed to dilate outcomes $k \in [n]$ to some PVM Π . Next lemma explains how to dilate a “leftover” POVM E related to Π in a certain way. This result will be used in Section 3.4.

Lemma 2.4. Let $\Pi := \{\Pi_i\}_{i=1}^n$ be a PVM on a Hilbert space \mathcal{H} and let G be a positive semidefinite operator on \mathcal{H} such that $G \preceq I_{\mathcal{H}}$. Suppose that there is also a POVM $E := \{E_i\}_{i=0}^n$ on \mathcal{H} defined as

$$E_i := \sqrt{G} \Pi_i \sqrt{G} \text{ for every } i \in [n], \quad E_0 := I_{\mathcal{H}} - G. \quad (39)$$

Then one can dilate the POVM E on \mathcal{H} to a PVM $\hat{\Pi} := \{\hat{\Pi}_i\}_{i=0}^n$ on $\hat{\mathcal{H}} := \mathbb{C}^2 \otimes \mathcal{H}$ as follows:

$$\hat{\Pi}_i := \begin{pmatrix} \sqrt{G} \Pi_i \sqrt{G} & -\sqrt{G} \Pi_i \sqrt{I_{\mathcal{H}} - G} \\ -\sqrt{I_{\mathcal{H}} - G} \Pi_i \sqrt{G} & \sqrt{I_{\mathcal{H}} - G} \Pi_i \sqrt{I_{\mathcal{H}} - G} \end{pmatrix} \quad \forall i \in [n], \quad \hat{\Pi}_0 := \begin{pmatrix} I_{\mathcal{H}} - G & \sqrt{G} \sqrt{I_{\mathcal{H}} - G} \\ \sqrt{G} \sqrt{I_{\mathcal{H}} - G} & G \end{pmatrix}. \quad (40)$$

³The statements regarding optimal POVMs for optimized resource states in the original papers [SSMH17; MSSH18] contain mistakes.

Proof. It is easy to see that the dilated PVM $\{\hat{\Pi}_i\}_{i=0}^n$ on $\hat{\mathcal{H}}$ has the form

$$\hat{\Pi}_i = U \begin{pmatrix} \Pi_i & 0 \\ 0 & 0 \end{pmatrix} U^\dagger \quad \forall i \in [n], \quad \text{and} \quad \hat{\Pi}_0 = U \begin{pmatrix} 0 & 0 \\ 0 & I_{\mathcal{H}} \end{pmatrix} U^\dagger, \quad (41)$$

where the unitary U is defined as

$$U := \begin{pmatrix} \sqrt{G} & -\sqrt{I_{\mathcal{H}} - G} \\ \sqrt{I_{\mathcal{H}} - G} & \sqrt{G} \end{pmatrix}. \quad (42)$$

It is easy to see that $\hat{\Pi}_i^2 = \hat{\Pi}_i = \hat{\Pi}_i^\dagger$ for every i and $\sum_{i=0}^n \hat{\Pi}_i = I_{\hat{\mathcal{H}}}$. Therefore $\hat{\Pi}$ is indeed a PVM on $\hat{\mathcal{H}}$. This PVM manifestly acts on vectors $|0\rangle \otimes |\psi\rangle \in \hat{\mathcal{H}}$ in the same way as the POVM E acts on $|\psi\rangle \in \mathcal{H}$, so it is indeed a Naimark's dilation of the POVM E . \square

Now we explain how to implement a PVM of a certain form, which we will later use in Section 3.3, assuming one can efficiently implement unitaries which define this PVM. Namely, assume that we have a PVM $\Pi = \{\Pi_k\}_{k=0}^n$ on $\mathcal{H} := \mathcal{H}_1 \otimes \mathcal{H}_2$ for some Hilbert spaces $\mathcal{H}_1, \mathcal{H}_2$ such that

$$\Pi_k := U_k \Pi_n U_k^\dagger \quad \text{for every } k \in [n] \quad (43)$$

$$\Pi_n := I_{\mathcal{H}_1} \otimes (W|0\rangle\langle 0|W^\dagger)_{\mathcal{H}_2} \quad (44)$$

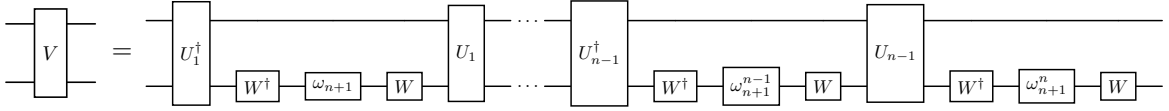
where $U_n := I_{\mathcal{H}}$, and we assume that all U_k are some easy-to-implement unitaries on $\mathcal{H} = \mathcal{H}_1 \otimes \mathcal{H}_2$, W is some easy-to-implement unitary on \mathcal{H}_2 and $|0\rangle$ is a computational basis vector on \mathcal{H}_2 .

We can implement the PVM Π as follows:

- Define a unitary V on \mathcal{H} as

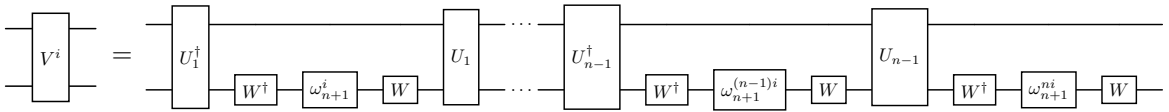
$$V := \sum_{k=0}^n \omega_{n+1}^k \Pi_k, \quad (45)$$

where ω_{n+1} is root of unity of order $n+1$. Observe, that we can implement the unitary V efficiently thanks to our assumptions via the following circuit on $\mathcal{H} = \mathcal{H}_1 \otimes \mathcal{H}_2$:

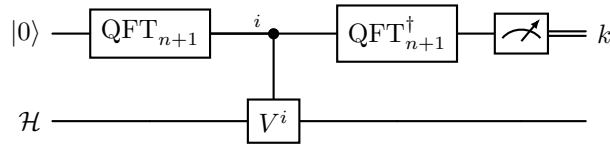


The gate ω_{n+1}^k represents the operator $\omega_{n+1}^k |0\rangle\langle 0| + (I - |0\rangle\langle 0|)$ on \mathcal{H}_2 . We also used $U_n = I_{\mathcal{H}}$.

- Note that implementing V^i is also easy:



- Now we can run the phase estimation circuit to measure the given register \mathcal{H} according to the PVM Π :



3. EFFICIENT QUANTUM ALGORITHMS FOR PBT IN STANDARD ENCODING

3.1. The standard PGM in the Gelfand–Tsetlin basis. Before presenting our PBT circuit, we need to explain how to dilate the POVM E from eq. (27) to a projective measurement Π . In principle, that is possible for any POVM due to *Naimark's dilation* theorem. However, in general it is not obvious how to achieve a conceptually simple dilation that can be efficiently implemented. We first explain how to construct such dilation explicitly, and then in Section 3.3 present an efficient circuit for E .

Due to eq. (13) the generator σ_n in the Gelfand–Tsetlin basis of any irrep $(\lambda, \varnothing) \in \hat{\mathcal{A}}_{n,1}^d$ can be written as

$$\psi_{(\lambda, \varnothing)}(\sigma_n) = \sum_{S \in \text{Paths}_{n-1}(\lambda, \varnothing)} |v_{S,\lambda}\rangle \langle v_{S,\lambda}|, \quad \text{where} \quad |v_{S,\lambda}\rangle := \sum_{a \in \text{AC}_d(\lambda)} \sqrt{\frac{m_{\lambda \cup a}}{m_\lambda}} |S \circ (\lambda \cup a) \circ (\lambda, \varnothing)\rangle \quad (46)$$

and $\psi_{(\mu, \square)}(\sigma_n) = 0$ for every $(\mu, \square) \in \widehat{\mathcal{A}}_{n,1}^d$. Also note that due to [GBO23, Lemma B.1] for every $\lambda \vdash_d n - 1$ and $a \in \text{AC}(\lambda)$ we have

$$n \cdot \frac{d_\lambda}{m_\lambda} \cdot \frac{m_{\lambda \cup a}}{d_{\lambda \cup a}} = d + \text{cont}(a). \quad (47)$$

Using eqs. (30), (46) and (47), we can rewrite E_n from eq. (29) in the Gelfand–Tsetlin basis of irrep $\Lambda = (\lambda, \varnothing) \in \widehat{\mathcal{A}}_{n,1}^d$ as follows:

$$\psi_{(\lambda, \varnothing)}(E_n) = \psi_{(\lambda, \varnothing)}(\rho^{-1/2} \sigma_n \rho^{-1/2}) = \sum_{S \in \text{Paths}_{n-1}(\lambda, \mathcal{B})} (\psi_{(\lambda, \varnothing)}(\rho))^{-1/2} |v_{S, \lambda}\rangle \langle v_{S, \lambda}| (\psi_{(\lambda, \varnothing)}(\rho))^{-1/2} \quad (48)$$

$$= \sum_{S \in \text{Paths}_{n-1}(\lambda, \mathcal{B})} |w_{S, \lambda}\rangle \langle w_{S, \lambda}|, \quad (49)$$

where we define for $\lambda \vdash_d n - 1$ and $S \in \text{Paths}_{n-1}(\lambda, \mathcal{B})$ we defined a vector $|v_{S, \lambda}\rangle$ in the irrep $(\lambda, \varnothing) \in \widehat{\mathcal{A}}_{n,1}^d$ as

$$|w_{S, \lambda}\rangle := \sum_{a \in \text{AC}_d(\lambda)} \sqrt{\frac{d_{\lambda \cup a}}{n \cdot d_\lambda}} |S \circ (\lambda \cup a) \circ (\lambda, \varnothing)\rangle. \quad (50)$$

3.2. Naimark’s dilation of the standard PGM. Recall that the Bratteli diagram of the symmetric group is the *Young lattice*⁴ [Sag13], and the following identity holds for every $\lambda \vdash n - 1$ [Sta13] in the Young lattice:

$$n \cdot d_\lambda = \sum_{a \in \text{AC}(\lambda)} d_{\lambda \cup a}, \quad (51)$$

where the notation $\lambda \cup a$ denotes the Young diagram in the Young lattice obtained by adding a box a to λ , and d_λ is the dimension of the symmetric group irrep λ .⁵

The main observation of this section is that for a Young diagram $\lambda \vdash n - 1$, we have $\text{AC}_d(\lambda) = \text{AC}(\lambda)$ if $\lambda_d = 0$ and $\text{AC}_d(\lambda) \neq \text{AC}(\lambda)$ if $\lambda_d > 0$. In particular, when $\lambda_d = 0$ this implies that

$$\| |w_{S, \lambda}\rangle \|^2 = \sum_{a \in \text{AC}_d(\lambda)} \frac{d_{\lambda \cup a}}{n \cdot d_\lambda} = \sum_{a \in \text{AC}(\lambda)} \frac{d_{\lambda \cup a}}{n \cdot d_\lambda} = 1, \quad (52)$$

so $\psi_{(\lambda, \varnothing)}(E_n)$ is an orthogonal projector. Since the cyclic shift π acts unitarily, all $\psi_{(\lambda, \varnothing)}(E_i)$ are orthogonal projectors as well. Because E provides a resolution of the identity in the irreducible representation $(\lambda, \varnothing) \in \widehat{\mathcal{A}}_{n,1}^d$, the POVM E restricted to the irreducible representation (λ, \varnothing) with $\lambda_d = 0$ is actually a PVM there. We will replace $\psi_{(\lambda, \varnothing)}(E_n)$ by $\psi_{(\lambda, \varnothing)}(\Pi_n)$ from now on to indicate that E is actually a PVM on $(\lambda, \varnothing) \in \widehat{\mathcal{A}}_{n,1}^d$.

However, for the irreps λ with $\lambda_d > 0$ the POVM E^λ is not a PVM because $\text{AC}(\lambda) = \text{AC}_d(\lambda) \sqcup \{(d+1, 1)\}$ and the vectors $|w_{S, \lambda}\rangle$ are not normalized anymore:

$$\| |w_{S, \lambda}\rangle \|^2 = \sum_{a \in \text{AC}_d(\lambda)} \frac{d_{\lambda \cup a}}{n \cdot d_\lambda} = \left(\sum_{a \in \text{AC}(\lambda)} \frac{d_{\lambda \cup a}}{n \cdot d_\lambda} \right) - \frac{d_{\lambda \cup (d+1, 1)}}{n \cdot d_\lambda} = 1 - \frac{d_{\lambda \cup (d+1, 1)}}{n \cdot d_\lambda} < 1, \quad (53)$$

where $\lambda \cup (d+1, 1)$ denotes the Young diagram obtained from λ by adding a cell with coordinates $(d+1, 1)$, so that $\ell(\lambda \cup (d+1, 1)) = d+1$. The vertex corresponding to this Young diagram does not exist in the Bratteli diagram \mathcal{B} . Fortunately, eq. (53) suggests immediately how to construct a Naimark’s dilation Π^λ of E^λ for λ with $\lambda_d > 0$. For this construction, one needs to modify the Bratteli diagram \mathcal{B} by adding vertices to each level $\geq n$. Then the set of all paths in this modified Bratteli diagram will define a new basis for the Naimark dilated Hilbert space.⁶

More concretely, to each level $k \leq p$ of the Bratteli diagram \mathcal{B} we add all possible vertices labelled by all Young diagrams $\nu \vdash k$ such that $\nu_{d+1} = 1$. An edge between a pair of Young diagrams in two consecutive levels is added if the latter diagram can be obtained by adding a cell to the previous one. This procedure ensures that all the levels up to n of the new Bratteli diagram form a subset of the Young lattice, such that for every vertex at level n the irrep dimensions still satisfy eq. (51). We call the new Bratteli diagram $\widetilde{\mathcal{B}}$. The basis for the Naimark dilated Hilbert space for the irrep $\Lambda \in \widehat{\mathcal{A}}_{n,1}^d$ consists of all paths from the root to the leaf Λ in this modified Bratteli diagram, which we denote by $\text{Paths}(\Lambda, \widetilde{\mathcal{B}})$. Formally, for every $\Lambda \in \widehat{\mathcal{A}}_{n,1}^d$, if $\Lambda = (\lambda, \varnothing)$ for $\lambda \vdash n - 1$, $\ell(\lambda) \geq d$ we define

$$\text{Paths}(\Lambda, \widetilde{\mathcal{B}}) := \left\{ T = (T^0, T^1, \dots, T^n, \Lambda) \in \widehat{\mathcal{A}}_{1,0}^{d+1} \times \dots \times \widehat{\mathcal{A}}_{n,0}^{d+1} \times \widehat{\mathcal{A}}_{n,1}^d \mid T \text{ satisfies eq. (55)} \right\}, \quad (54)$$

⁴Sometimes Young lattice is also called *Young graph*. Young graph usually includes all possible partitions $\nu \vdash k$ at a given level k . However, our Bratteli diagram \mathcal{B} up to level n coincides with a subset of the Young graph: only the partitions $\nu \vdash k$ with $\ell(\nu) \leq d$ are included in our \mathcal{B} .

⁵The dimension d_λ can be both understood as the number of paths from the root to a vertex λ in the Young lattice as well as in the Bratteli diagram of $\widehat{\mathcal{A}}_{n,0}^d$, since up to level n the Bratteli diagram is a subset of the full Young lattice and the procedure of adding a cell is monotonic with respect to the number of rows in λ along a given path in the Young lattice.

⁶We have provided a *Wolfram Mathematica* notebook implementing our construction on [GitHub](#).

where

$$T_{d+1}^k \leq 1 \quad \forall k \in [n], \text{ and } T^{k-1} \rightarrow T^k \quad \forall k \in [n], \text{ and } T^n = \lambda \cup a \text{ for some } a \in \text{AC}(\lambda). \quad (55)$$

If $\Lambda_r \neq \emptyset$ then

$$\text{Paths}(\Lambda, \tilde{\mathcal{B}}) := \text{Paths}(\Lambda, \mathcal{B}). \quad (56)$$

This extension of the Bratteli diagram is illustrated in Fig. 1.

The action $\tilde{\psi}_\Lambda$ of the transposition generators $\sigma_1, \dots, \sigma_{n-1}$ of $\mathcal{A}_{n,1}^d$ in this dilated Bratteli diagram $\tilde{\mathcal{B}}$ is given by the generalization of eq. (11) to all paths in $\text{Paths}(\Lambda, \tilde{\mathcal{B}})$, i.e. for every $T \in \text{Paths}(\Lambda, \tilde{\mathcal{B}})$ and every $i \in [n-1]$ we define:

$$\tilde{\psi}_\Lambda(\sigma_i) |T\rangle = \frac{1}{r_i(T)} |T\rangle + \sqrt{1 - \frac{1}{r_i(T)^2}} |\sigma_i T\rangle \quad \text{for } i \neq n. \quad (57)$$

For this new Bratteli diagram $\tilde{\mathcal{B}}$, we define the dilated versions $|\tilde{w}_{S,\lambda}\rangle$ of vectors $|w_{S,\lambda}\rangle$ for $S \in \text{Paths}_{n-1}(\lambda, \tilde{\mathcal{B}})$ as

$$|\tilde{w}_{S,\lambda}\rangle := \sum_{a \in \text{AC}(\lambda)} \sqrt{\frac{d_{\lambda \cup a}}{n \cdot d_\lambda}} |S \circ (\lambda \cup a) \circ (\lambda, \emptyset)\rangle. \quad (58)$$

Therefore in the dilated space since eq. (51) holds we have

$$\| |\tilde{w}_{S,\lambda}\rangle \|^2 = \sum_{a \in \text{AC}(\lambda)} \frac{d_{\lambda \cup a}}{n \cdot d_\lambda} = 1. \quad (59)$$

More importantly, we have the following

Lemma 3.1. *For every $\Lambda = (\lambda, \emptyset)$ in the dilated Hilbert space spanned by $\text{Paths}(\Lambda, \tilde{\mathcal{B}})$ we have*

$$\sum_{k=1}^n \sum_{S \in \text{Paths}_{n-1}(\lambda, \tilde{\mathcal{B}})} \tilde{\psi}_\Lambda(\pi^k) |\tilde{w}_{S,\lambda}\rangle \langle \tilde{w}_{S,\lambda} | \tilde{\psi}_\Lambda(\pi^{-k}) = I \quad (60)$$

Proof. Denote

$$A := \sum_{k=1}^n \sum_{S \in \text{Paths}_{n-1}(\lambda, \tilde{\mathcal{B}})} \tilde{\psi}_\Lambda(\pi^k) |\tilde{w}_{S,\lambda}\rangle \langle \tilde{w}_{S,\lambda} | \tilde{\psi}_\Lambda(\pi^{-k}). \quad (61)$$

Note that by construction eq. (57) any $\sigma \in S_{n-1}$ (we think of σ as an element of the algebra $\mathcal{A}_{n-1,0}^d$) acts irreducibly on $\text{Paths}(\Lambda, \tilde{\mathcal{B}})$, i.e.

$$\sum_{S \in \text{Paths}_{n-1}(\lambda, \tilde{\mathcal{B}})} |\tilde{w}_{S,\lambda}\rangle \langle \tilde{w}_{S,\lambda} | \tilde{\psi}_\Lambda(\sigma) = \tilde{\psi}_\Lambda(\sigma) \sum_{S \in \text{Paths}_{n-1}(\lambda, \tilde{\mathcal{B}})} |\tilde{w}_{S,\lambda}\rangle \langle \tilde{w}_{S,\lambda} |. \quad (62)$$

Therefore A must commute with $\mathcal{A}_{n,0}^d$ since π^k are transversals for cosets of $\mathcal{A}_{n,0}^d$ over $\mathcal{A}_{n-1,0}^d$:

$$A = \frac{1}{(n-1)!} \sum_{\sigma \in S_{n-1}} \sum_{k=1}^n \sum_{S \in \text{Paths}_{n-1}(\lambda, \tilde{\mathcal{B}})} \tilde{\psi}_\Lambda(\pi^k \sigma) |\tilde{w}_{S,\lambda}\rangle \langle \tilde{w}_{S,\lambda} | \tilde{\psi}_\Lambda((\pi^k \sigma)^{-1}) \quad (63)$$

$$= \frac{1}{(n-1)!} \sum_{\sigma \in S_n} \sum_{S \in \text{Paths}_{n-1}(\lambda, \tilde{\mathcal{B}})} \tilde{\psi}_\Lambda(\sigma) |\tilde{w}_{S,\lambda}\rangle \langle \tilde{w}_{S,\lambda} | \tilde{\psi}_\Lambda(\sigma^{-1}). \quad (64)$$

This means that A is a diagonal matrix and $\langle T | A | T \rangle$ depends only on T^n , so for every $a \in \text{AC}(\lambda)$ and every $T \in \text{Paths}(\Lambda, \tilde{\mathcal{B}})$ with $T^n = \lambda \cup a$ we can write

$$\langle T | A | T \rangle = \frac{1}{d_{\lambda \cup a}} \sum_{\substack{T \in \text{Paths}(\Lambda, \tilde{\mathcal{B}}) \\ T^n = \lambda \cup a}} \langle T | A | T \rangle = \frac{1}{d_{\lambda \cup a} (n-1)!} \sum_{\substack{S \in \text{Paths}_{n-1}(\lambda, \tilde{\mathcal{B}}) \\ T \in \text{Paths}(\Lambda, \tilde{\mathcal{B}}) \\ T^n = \lambda \cup a}} \sum_{\sigma \in S_n} \langle \tilde{w}_{S,\lambda} | \tilde{\psi}_\Lambda(\sigma^{-1}) | T \rangle \langle T | \tilde{\psi}_\Lambda(\sigma) | \tilde{w}_{S,\lambda} \rangle, \quad (65)$$

but in the above formula $\tilde{\psi}_\Lambda(\sigma)$ commutes with $\sum_T |T\rangle \langle T|$. Therefore,

$$\langle T | A | T \rangle = \frac{1}{d_{\lambda \cup a} (n-1)!} \sum_{\sigma \in S_n} \sum_{\substack{S \in \text{Paths}_{n-1}(\lambda, \tilde{\mathcal{B}}) \\ T \in \text{Paths}(\Lambda, \tilde{\mathcal{B}}) \\ T^n = \lambda \cup a}} |\langle T | \tilde{w}_{S,\lambda} \rangle|^2 = \frac{n \cdot d_\lambda}{d_{\lambda \cup a}} \frac{d_{\lambda \cup a}}{n \cdot d_\lambda} = 1. \quad (66)$$

Since every diagonal element of A is 1, so $A = I$. \square

Consequently, in the dilated space our POVM E becomes a PVM, which we denote by Π . From now on assume that we work in the dilated Gelfand–Tsetlin basis spanned by $T \in \text{Paths}(\Lambda, \tilde{\mathcal{B}})$ and we want to implement the PVM $\Pi = \{\Pi_k\}_{k=0}^n$, where for every $k \in [n]$:

$$\Pi_k := \pi^k \Pi_n \pi^{-k} \text{ and } \tilde{\psi}_{(\lambda, \emptyset)}(\Pi_n) = \sum_{S \in \text{Paths}_{n-1}(\lambda, \tilde{\mathcal{B}})} |\tilde{w}_{S, \lambda}\rangle \langle \tilde{w}_{S, \lambda}|, \quad \Pi_0 = I - \sum_{k=1}^n \Pi_k. \quad (67)$$

3.3. Quantum circuit for the standard PGM. Using the results of Section 3.2, our task now is to implement the PVM Π from eq. (67). We embed $\text{Paths}(\mathcal{B})$ in a Hilbert space with appropriate tensor product structure dictated by the mixed quantum Schur transform [GBO23]. Mixed quantum Schur transform can be implemented using two different encodings for the Gelfand–Tsetlin basis of $\mathcal{A}_{n,1}^d$: the *standard* encoding or the *Yamanouchi* encoding, see [GBO23] for more details. In this section, we discuss how to implement Π with the standard encoding. The Yamanouchi encoding implementation is explained in the Section 4.

Before presenting our circuit for Π , we need to define a unitary \tilde{W} acting on registers T^{n-1}, T^n, T^{n+1} , which can be used to prepare the states $|\tilde{w}_{S, \lambda}\rangle := |S\rangle |\tilde{w}_\lambda\rangle$ for every $(\lambda, \emptyset) \in \tilde{\mathcal{A}}_{n,1}^d$ and $S \in \text{Paths}(\Lambda, \tilde{\mathcal{B}})$. Namely, we first define

$$\tilde{W}_\lambda |0\rangle := |\tilde{w}_\lambda\rangle, \quad |\tilde{w}_\lambda\rangle := \sum_{a \in \text{AC}(\lambda)} \sqrt{\frac{d_{\lambda \cup a}}{n \cdot d_\lambda}} |\lambda \cup a\rangle, \quad (68)$$

where \tilde{W}_λ is a unitary matrix of size at most $(d+1) \times (d+1)$ with easy-to-compute entries $|\tilde{w}_\lambda\rangle$ in its first column. Now we define \tilde{W} , a controlled version of \tilde{W}_λ , as a unitary which prepares $|\tilde{w}_\lambda\rangle$ conditioned on λ :

$$\tilde{W} := \sum_{\lambda' \vdash_{d-1} n-1} \left(\left(\sum_{\substack{\lambda' \neq \lambda \\ \lambda' \vdash_{d-1} n-1}} |\lambda'\rangle \langle \lambda'| \right) \otimes I + |\lambda\rangle \langle \lambda| \otimes \tilde{W}_\lambda \right) \otimes |(\lambda, \emptyset)\rangle \langle (\lambda, \emptyset)| + \sum_{\mu \vdash_{d-1} n} I \otimes I \otimes |(\mu, \square)\rangle \langle (\mu, \square)|. \quad (69)$$

This transformation can be implemented via a sequence of Givens rotations. Similarly to eq. (68), we can define a unitary W_λ which prepares the normalized version of $|\tilde{w}_\lambda\rangle$:

$$W_\lambda |0\rangle := \frac{|\tilde{w}_\lambda\rangle}{\| |\tilde{w}_\lambda\rangle \|}, \quad |\tilde{w}_\lambda\rangle = \sum_{a \in \text{AC}_d(\lambda)} \sqrt{\frac{d_{\lambda \cup a}}{n \cdot d_\lambda}} |\lambda \cup a\rangle. \quad (70)$$

The gate W is now defined for eq. (70) in the same way as \tilde{W} in eq. (69).

Assume the initial state is $|S\rangle |0\rangle |\lambda\rangle := |S^2\rangle \dots |S^{n-2}\rangle |\lambda\rangle |0\rangle |(\lambda, \emptyset)\rangle$ for arbitrary $S \in \text{Paths}_{n-1}(\lambda, \tilde{\mathcal{B}})$, where $|0\rangle$ is some basis state of the register, corresponding to the n -th level of the dilated Bratteli diagram $\tilde{\mathcal{B}}$. Then we can prepare a state $|S\rangle |\tilde{w}_\lambda\rangle |(\lambda, \emptyset)\rangle$ as follows:

$$(I \otimes \tilde{W}) |S\rangle |0\rangle |\lambda\rangle = |S\rangle |\tilde{w}_\lambda\rangle |\lambda\rangle, \quad (71)$$

where identity I acts on the registers $|S^2\rangle \dots |S^{n-2}\rangle$. Moreover, note that the amplitudes of the state $|\tilde{w}_\lambda\rangle$ are easy to calculate on a classical computer in time $\tilde{O}(d)$ due to:

Lemma 3.2 ([Kos03]). *For every $\lambda \vdash n-1$ and $a \in \text{AC}(\lambda)$ there holds*

$$\frac{\prod_{c \in \text{RC}(\lambda)} (\text{cont}(a) - \text{cont}(c))}{\prod_{c \in \text{AC}(\lambda) \setminus a} (\text{cont}(a) - \text{cont}(c))} = \frac{d_{\lambda \cup a}}{n \cdot d_\lambda}. \quad (72)$$

Each \tilde{W}_λ gate can be implemented as a sequence of simple controlled R_i gates, as shown in Fig. 5, which we define as

$$R_i |0\rangle := \sqrt{\frac{1 - \sum_{j=1}^i \eta_j}{1 - \sum_{j=1}^{i-1} \eta_j}} |0\rangle + \sqrt{\frac{\eta_i}{1 - \sum_{j=1}^{i-1} \eta_j}} |1\rangle, \quad \eta_j := \frac{d_{\lambda \cup a_j}}{n \cdot d_\lambda} \quad (73)$$

where the cell $a_j \in \text{AC}(\lambda)$ is located in the j -th row of λ . If for a given j there is no such cell then the control on R_i in Fig. 5 is not triggered. In other words, R_i is triggered only when $\lambda_{i-1} > \lambda_i$ (R_1 is always triggered). Note that due to Lemma 3.2 the amplitudes in eq. (73) are easy to compute classically in time $\tilde{O}(d)$.

Following the prescription outlined above, we construct in Fig. 2 an efficient circuit for the PGM E dilated as Π . The circuit mainly acts on the dilated space spanned by $(T^0, T^1, T^2, \dots, T^n, T^{n+1}) \in \text{Paths}(\tilde{\mathcal{B}})$, which form the Gelfand–Tsetlin basis. The ancilla registers are used implicitly in the circuit.

First, a mixed quantum Schur transform maps the computational basis to the mixed Schur basis which is usually labelled by $|M_{[d-1]}, T\rangle$, where M is a Gelfand–Tsetlin pattern and T is a path in \mathcal{B} . We assume a tensor product structure for different vertices T^i of the path $T \in \text{Paths}(\mathcal{B})$ and we use the standard encoding for $|T\rangle$. Moreover, all registers T^2, \dots, T^n are assumed to be dilated, according to the procedure explained in Section 3.2. Since T^0 and T^1 can only have one possible value, we omit those registers from the diagram since they are one-dimensional. The last level T^{n+1} of the path T is labelled by λ and indicates an irreducible

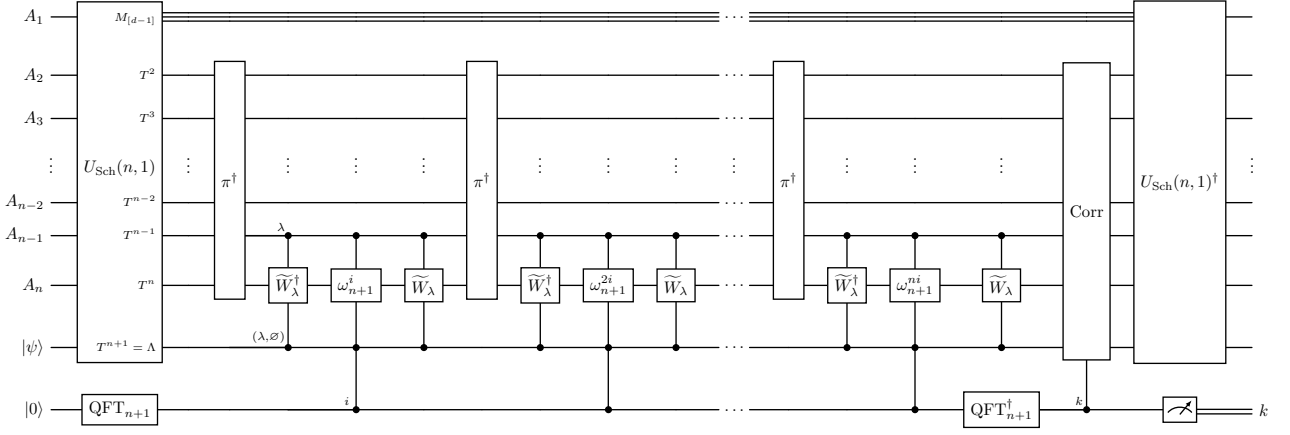


FIGURE 2. The circuit implementation of the PGM E (27) for dPBT in standard encoding. The registers T^2, T^3, \dots, T^n are dilated as per Section 3.2. The correction gate Corr together with $U_{\text{Sch}}(n, 1)^\dagger$ transform is optional: it is used to bring the post-measurement state to the form defined by the original PGM measurement E .

representation. The cyclic permutation gate $\pi = (12 \dots n) = \sigma_1 \sigma_2 \dots \sigma_{n-1}$ acts only on $n-1$ wires of the dilated Gelfand–Tsetlin basis, and each of the transpositions σ_i acts only locally on the registers T^{i-1}, T^i, T^{i+1} (σ_1 acts only on T^2 , and σ_2 acts only on T^2, T^3). \widetilde{W} prepares the state $|\widetilde{w}_\lambda\rangle$ conditioned on λ , i.e., $\widetilde{W}_\lambda|0\rangle = |\widetilde{w}_\lambda\rangle$ where \widetilde{W}_λ is controlled on λ . The phase gates ω_{n+1}^{ki} act non-trivially only on $|0\rangle$ in the register T^n , and are controlled on the condition $T^{n-1} = T^{n+1} = \lambda$. Finally, the measurement outcome $k = 0$ corresponds to the failure of the protocol, otherwise $k \in [n]$ indicates the port where Bob can find the teleported state $|\psi\rangle$ of dimension d .

We now argue that the gate complexity of our circuit in Fig. 2 is $\widetilde{O}(nd^4)$:

- (1) The complexity of implementing the mixed quantum Schur transform $U_{\text{Sch}}(n, 1)$ is $\widetilde{O}(nd^4)$ [Ngu23; GBO23].
- (2) The complexity of implementing $\pi = \sigma_1 \sigma_2 \dots \sigma_{n-1}$ based on Fig. 3 is $\widetilde{O}(nd^2)$. The factor n comes from the number of transpositions σ_i in π . Each transposition σ_i is 3-local: it acts only on registers T^{i-1}, T^i, T^{i+1} . More specifically, σ_i is a 2×2 rotation on T^i controlled by T^{i-1} and T^{i+1} . According to Fig. 4, each σ_i can be implemented with $\widetilde{O}(d^2)$ gates, each of which decompose into $\widetilde{O}(1)$ elementary gates. In particular, each of the $R_{j,k}$ gates

$$R_{j,k} := \begin{pmatrix} \frac{1}{r_{j,k}} & \sqrt{1 - \frac{1}{r_{j,k}^2}} \\ \sqrt{1 - \frac{1}{r_{j,k}^2}} & -\frac{1}{r_{j,k}} \end{pmatrix}, \quad r_{j,k} := \lambda_j - \lambda_k + k - j \quad (74)$$

appearing in Fig. 4 can be implemented with $\widetilde{O}(1)$ elementary gates and $\widetilde{O}(1)$ auxiliary qubits for computation of rotation parameters $r_{j,k}$.

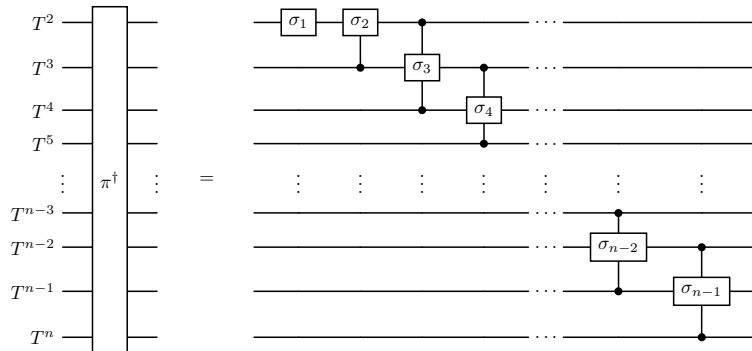


FIGURE 3. Circuit for the cyclic permutation $\pi^\dagger = \sigma_{n-1} \sigma_{n-2} \dots \sigma_2 \sigma_1$ in the Gelfand–Tsetlin basis. Each transposition σ_i acts locally on registers T^{i-1}, T^i, T^{i+1} , with T^{i-1} and T^{i+1} used as controls. Note, that σ_1 acts only on T^2 , and σ_2 acts only on T^2, T^3 because we have dropped the registers T^0, T^1 (they are always one-dimensional).

- (3) The operation \widetilde{W} defined in eq. (69) is a λ -controlled unitary \widetilde{W}_λ that acts non-trivially only on a $(d+1)$ -dimensional subspace of the register T^n . This register consists of $d+1$ wires corresponding to $d+1$ rows of a Young diagram, see Fig. 5. The matrix entries of \widetilde{W}_λ (see eq. (68)) can be reversibly computed on the fly

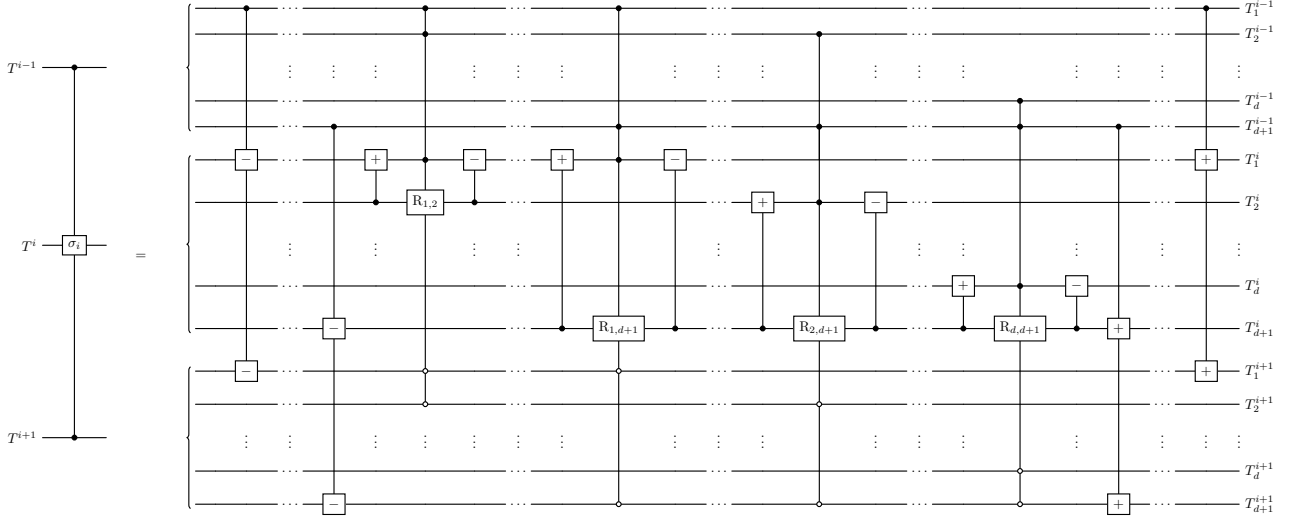


FIGURE 4. Quantum circuit for implementing the transposition σ_i in the Gelfand–Tsetlin basis. The controlled “ \pm ” gates perform arithmetic operations that add / subtract the control register from the target registers. For each j, k such that $1 \leq j < k \leq d$, the corresponding $R_{j,k}$ gate defined in eq. (74) acts on the k -th register of T^i and has five controls: the j -th and k -th registers of T^{i-1} and T^{i+1} , and the j -th register of T^i . At this level of abstraction, the implementation of σ_i contains $\tilde{O}(d^2)$ gates.

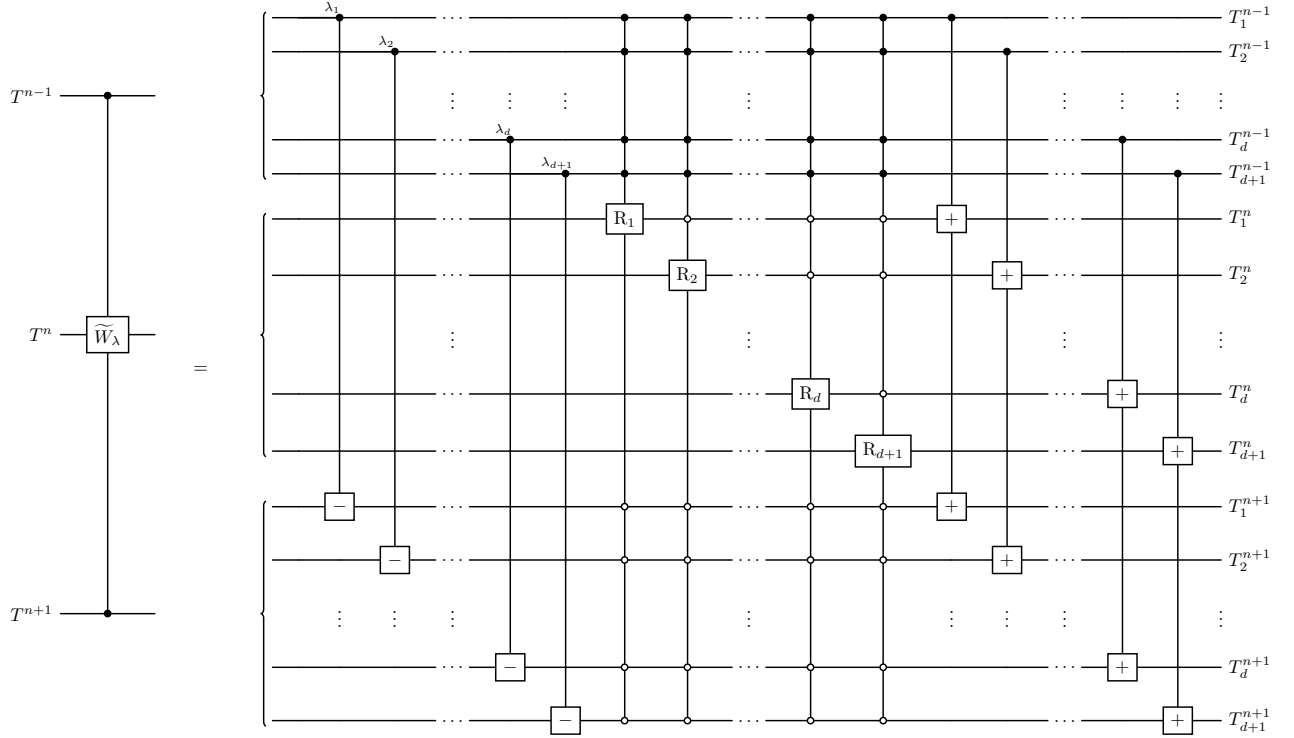


FIGURE 5. Quantum circuit for implementing the unitary \tilde{W} defined by (69) in the Gelfand–Tsetlin basis. The controlled “ \pm ” gates perform arithmetic operations that add / subtract the control register from the target registers, just as on Fig. 4. eq. (74) defines rotation gates R_j that are controlled on $2(d+1+j)$ registers in total: all registers of T^{i-1} and T^{i+1} and first $(j-1)$ registers of T^i . The overall gate complexity of \tilde{W} is $\tilde{O}(d^2)$.

using gates R_i , $i \in [d+1]$ from eq. (73) in classical time $\tilde{O}(d)$, which must be implemented in a quantum circuit coherently. Therefore, implementing \tilde{W} would have the gate complexity $\tilde{O}(d^2)$.

- (4) ω_{n+1}^{ki} denotes the gate $\omega_{n+1}^{ki}|0\rangle\langle 0| + (I - |0\rangle\langle 0|)$ on register T^n conditioned on the registers $T^{n-1} = \lambda$, $T^{n+1} = \Lambda = (\lambda, \emptyset)$. This has complexity $\tilde{O}(1)$.
- (5) The complexity of the Quantum Fourier Transform QFT_{n+1} is $\tilde{O}(1)$.

- (6) One can optionally implement the correction gate Corr together with inverse mixed Schur transform at the end to get the right post-measurement state (according to the definition of PGM E from eq. (27)). For that one needs to uncompute the gates π^k for $k \in [n]$ and \widetilde{W}_λ , and instead run the gate W_λ from eq. (69) followed by π^k . The complexity of implementing the correction gate does not change both the total gate and time complexities of the full circuit, adding only a constant factor overhead.

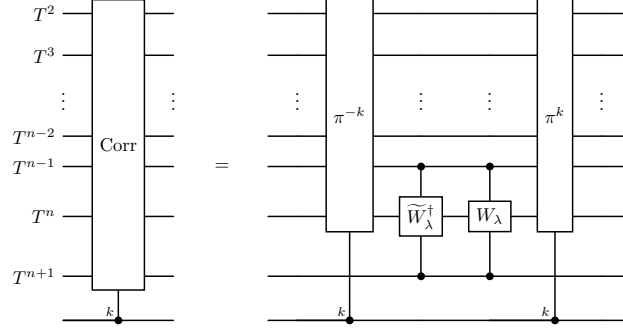


FIGURE 6. Circuit for the correction operation Corr. W_λ gate is defined in eq. (69) and its implementation is completely analogous to \widetilde{W}_λ from Fig. 5.

- (7) Now we are ready to count the total gate and time complexity. For that, notice that each gate π^\dagger in Fig. 2 consisting of local gates σ_i as in Fig. 3 can be pushed to the left of the circuit. This will reduce the naive complexity $\widetilde{O}(n^2 d^2)$ of implementing n sequential gates π^\dagger to just $\widetilde{O}(nd^2)$. Counting everything together gives $\widetilde{O}(nd^4)$ total time complexity. The gate complexity is $\widetilde{O}(n^2 d^4)$.

Similarly, we can count the number of auxiliary qubits needed to implement our circuit Fig. 2 in the standard encoding. However, we must be careful with the precision of implementing each gate. If the total target precision is ϵ then if the circuit has $\text{poly}(n, d)$ gates it implies the precision per each gate must be $\epsilon_g := \epsilon / \text{poly}(n, d)$. This will translate into the size of auxiliary registers for classical computation of matrix entries of the unitaries which need to be implemented coherently: the number of qubits needed for such computations will scale as $\log(1/\epsilon_g) = O(\log(1/\epsilon) + \log(n) + \log(d))$. With that in mind, we can summarize the total space complexity:

- (1) The number of auxiliary qubits needed to implement the mixed Schur transform isometry in the standard encoding [GBO23] and create a Naimark's dilation from Section 3.2 after the mixed Schur transfer is $(n + d)d \log(n) \text{polylog}(d, 1/\epsilon)$.
- (2) The number of auxiliary qubits needed to implement each gate σ_i from Fig. 4 inside π^\dagger gate from Fig. 3 is $\log(n) \text{polylog}(d, 1/\epsilon)$. However, when $O(n)$ gates σ_i are implemented in parallel with the shift trick of π^\dagger gates we need to have $n \log(n) \text{polylog}(d, 1/\epsilon)$ auxiliary qubits available.
- (3) The gates \widetilde{W}_λ and W_λ require $d^2 \log(n) \text{polylog}(d, 1/\epsilon)$ qubits to implement gates R_i , see Fig. 5.
- (4) Overall, the total number of auxiliary qubits needed is $(n + d)d \log(n) \text{polylog}(d, 1/\epsilon)$.

The above analysis finishes the proof of the first statement of Theorem 1.1 for standard PGM. In the next section, we describe how to extend the construction for standard PGM for generic PBT measurements, including the measurement needed to implement pPBT with the EPR resource state.

3.4. Efficient quantum algorithms for generic PBT measurements. It is straightforward now to extend the quantum circuit for the standard PGM Fig. 2 to quantum circuits for pPBT POVM from eqs. (33), (34), (37) and (38). For that, we can employ Lemma 2.4 for each irrep $(\lambda, \varnothing) \in \widehat{\mathcal{A}}_{n,1}^d$, where $\widetilde{\psi}_{(\lambda, \varnothing)}(U)$ is determined by the corresponding diagonal matrix G from eq. (37) extended to Naimark dilated space as $\langle T | \widetilde{\psi}_{(\lambda, \varnothing)}(G) | T \rangle = 0$ for all $T \in \text{Paths}(\Lambda, \widetilde{\mathcal{B}}) \setminus \text{Paths}(\Lambda, \mathcal{B})$. We introduce an additional qubit on which we would act with a unitary $U_{\lambda,a}$ depending on the irrep $(\lambda, \varnothing) \in \widehat{\mathcal{A}}_{n,1}^d$ and $a \in \text{AC}(\lambda)$:

$$U_{\lambda,a} = \begin{pmatrix} \sqrt{G_{\lambda,a}} & -\sqrt{1 - G_{\lambda,a}} \\ \sqrt{1 - G_{\lambda,a}} & \sqrt{G_{\lambda,a}} \end{pmatrix}, \quad (75)$$

where $G_{\lambda,a}$ are defined in eqs. (37) and (38) for pPBT with EPR resource state. The resulting circuit Fig. 7 is almost the same as Fig. 2. The complexity of computing $G_{\lambda,a}$ classically is $\widetilde{O}(1)$. Therefore the time, gate and space complexities of the circuit Fig. 7 are the same as for Fig. 2. Note that our construction works for any diagonal matrix $\psi_\Lambda(G)$ as long as its diagonal entries $G_{\lambda,a}$ are efficiently classically computable. The correction gate Corr in Fig. 2 is implemented in the same way as in Fig. 6, except one needs to uncompute $U_{\lambda,a}$ on the additional qubit register and do the uncomputation conditioned on the outcome $k = 0$.

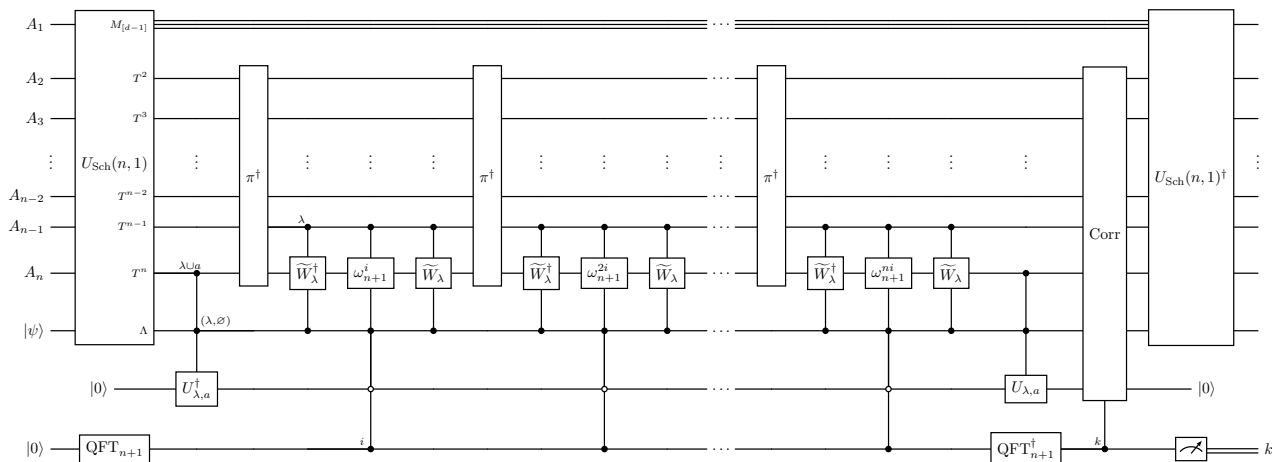


FIGURE 7. The circuit implementation of the PGM for pPBT in standard encoding. Notice that the circuit is almost the same as the one for dPBT presented on Fig. 2. The only difference is an additional register and a controlled rotation matrix (75).

3.5. Exponentially improved lower bound for non-local quantum computation. Port-based teleportation has interesting applications in holography and non-local quantum computation [May19; May22], where it was argued that the complexity of the local operation controls the amount of entanglement needed to implement it non-locally, using ideas from AdS/CFT correspondence. In particular, it was derived in [May22, Lemma 9] that port-based teleportation can be used to lower bound the amount of entanglement needed to implement a given channel (from a large class of one-sided quantum channels) non-locally in terms of the so-called *interaction-class circuit complexity* [May22, Definition 3] denoted by \mathcal{C} :

$$\Omega(\log \log \mathcal{C}) \leq E_c, \quad (76)$$

where E_c is the entanglement cost needed to implement non-locally a unitary with complexity \mathcal{C} , see [May22, Equation 29]. Port-based teleportation can also be used to find an upper bound [BK11; Spe16; May22]. The derivation of the lower bound uses a trivial upper bound $\exp(O(p))$ for the complexity of the port-based teleportation in terms of the number of ports n , see [May22, Equation 47]. It is already pointed out in [May22, page 28] that a better implementation of the port-based teleportation protocol would lead to a better lower bound. Complexities of our implementations of PBT protocols are $\tilde{O}(nd^4)$, therefore this immediately translates, according to [May22, Lemma 9], to a better lower bound:

$$\Omega(\log \mathcal{C}) \leq E_c, \quad (77)$$

thus improving exponentially upon the previous known bound.

4. LOGARITHMIC SPACE PBT VIA YAMANOUCHI ENCODING

Using the Yamanouchi encoding possibility of the mixed quantum Schur transform [GBO23] defined in eq. (22), it is possible to reduce the space complexity of the constructions presented in Section 3.3 from $O(n \log(n))$ to $O(\log(n))$. The resulting circuits for generic PBT measurements, including standard PGM and the POVM for EPR resource state pPBT, are presented in Fig. 8. They look essentially the same as Fig. 7 except for the differences in implementation of gates π^\dagger , σ_i and \tilde{W}_λ which stem from the different type of encoding.

Similarly to Section 3.3 we can count the total gate and time complexities in Fig. 8 as follows:

- (1) The complexity of implementing the mixed quantum Schur transform $U_{\text{Sch}}(n, 1)$ in Yamanouchi encoding is $\tilde{O}(nd^4)$ [GBO23].
- (2) The complexity of implementing $\pi = \sigma_1 \sigma_2 \dots \sigma_{n-1}$ based on Fig. 9 is $\tilde{O}(nd^2)$. The factor n comes from the number of transpositions σ_i in π , which are implemented sequentially.
- (3) Each transposition σ_i is more tricky in Yamanouchi encoding, see Figs. 10 and 11. More specifically, to implement σ_i we need to obtain the full information about the Young diagram T^{i-1} by using an auxiliary space and recording the description of T^{i-1} sequentially from registers y_k for $k < i$ via a Rec_k gates, see Fig. 10. Now, according to Fig. 11, each σ_i can be implemented with $\tilde{O}(d^2)$ gates $R_{i,j}$ from eq. (74), acting on wires y_i, y_{i+1} each of which decompose into $\tilde{O}(1)$ elementary gates and $\tilde{O}(1)$ auxiliary qubits for computation of rotation parameters $r_{j,k}$.
- (4) The operation \tilde{W} defined in eq. (69) is implemented similarly to Fig. 5 and the recording procedure described in Fig. 10. The time and gate complexities for that are $\tilde{O}(nd^2)$.

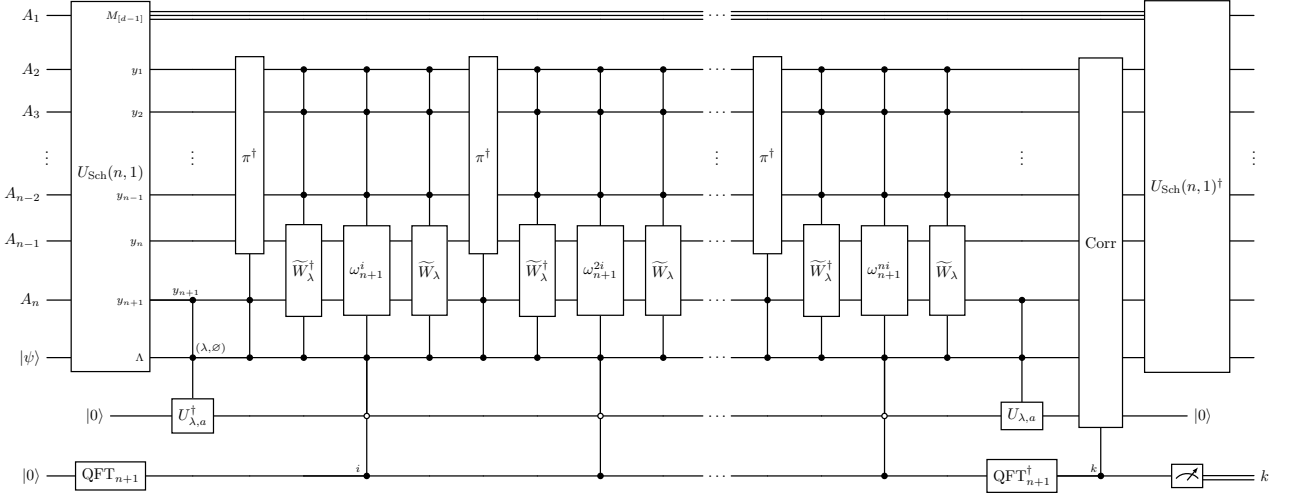


FIGURE 8. The circuit implementation of the PGM for pPBT in Yamanouchi encoding. Notice that the structure of the circuit is exactly the same as with standard encoding, see Fig. 7, except that wires T^2, \dots, T^n containing information about path $T = (T^0, \dots, T^n)$ via standard encoding are replaced by wires y_1, \dots, y_{n+1} which contain the same information via Yamanouchi encoding. This is obtained by another form of mixed Schur isometry, see eq. (23). This requires reformulation for all subsequent gates from the standard to Yamanouchi encoding, which we present on Figs. 9 to 11.

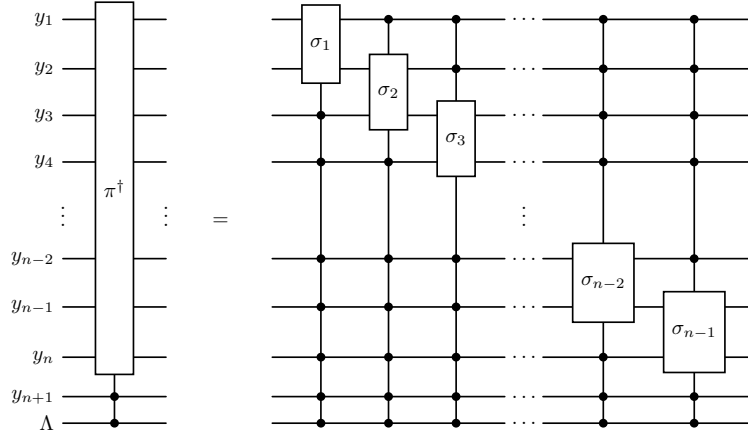


FIGURE 9. Quantum circuit for the cyclic permutation $\pi^\dagger = \sigma_{n-1}\sigma_{n-2}\cdots\sigma_2\sigma_1$ in the Yamanouchi encoding. Each transposition σ_i acts locally on registers y_i and y_{i+1} , while being controlled on all other registers y_i and Λ . Note that in standard encoding, σ_i was controlled only on two registers, compare with Fig. 3. Fig. 10 presents the exact form of a transposition σ_i gate in Yamanouchi encoding.

- (5) The implementation of ω_{n+1}^{ki} has complexity $\tilde{O}(n)$.
- (6) The complexity of the Quantum Fourier Transform QFT_{n+1} is $\tilde{O}(1)$.
- (7) One can optionally implement the correction gate Corr together with inverse mixed Schur transform at the end to get the right post-measurement state as in Fig. 7. The complexity of implementing this does not change both the total gate and time complexities of the full circuit, adding only a constant factor overhead.
- (8) Overall, counting everything together gives $\tilde{O}(n^2 d^4)$ for both total gate and time complexities in Yamanouchi encoding: essentially all nontrivial operations run sequentially.

Similarly, we can count the number of auxiliary qubits needed to implement our circuit Fig. 2 in the Yamanouchi encoding similarly to Section 3.3:

- (1) The number of auxiliary qubits needed to implement the mixed Schur transform isometry in the standard encoding [GBO23] and create a Naimark's dilation from Section 3.2 after the mixed Schur transfer is $d^2 \log(n)$ polylog($d, 1/\epsilon$). One important technical remark regarding Figs. 8 to 11 is that we do not depict an additional qudit of dimension $n+1$ which is needed to extend the Bratteli diagram from \mathcal{B} to $\tilde{\mathcal{B}}$ according to Section 3.2: it extends the space of Yamanouchi words on alphabet $[d]$ to the space of Yamanouchi words

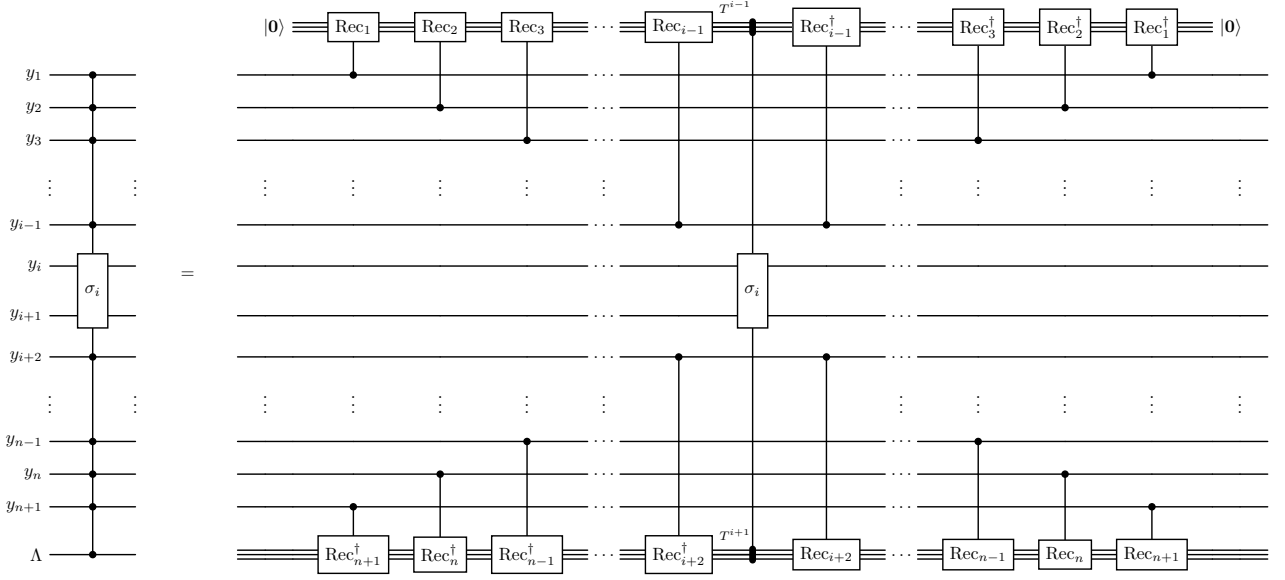


FIGURE 10. Quantum circuit for implementing a transposition σ_i in the Yamanouchi encoding. To correctly compute the rotation angles, we shall recover the information about parts T^{i-1} and T^{i+1} of a path T from its form in Yamanouchi encoding. This is achieved by a sequence of recording gates Rec_i performed on two auxiliary registers and controlled on y_i register. After recovering information about T^{i-1} and T^{i+1} , transposition σ_i can be simply performed as presented on Fig. 11.

with at most one symbol $d + 1$ among y_1, \dots, y_n by encoding the location i of the value $d + 1$ among y_1, \dots, y_n (if there exist i such that $y_i = d + 1$ then it also must be $y_{n+1} = d + 1$). Incorporation of this qubit is trivial and it does not change the time and gate complexities, however, the depiction of it is not convenient, so we omit it.

- (2) The number of auxiliary qubits needed to implement each gate separately σ_i from Fig. 11 is $\log(n)$ polylog($d, 1/\epsilon$). We implement all gates σ_i sequentially in the Yamanouchi encoding so we can reuse $\log(n)$ polylog($d, 1/\epsilon$) auxiliary qubits for each gate.
- (3) The gates \widetilde{W}_λ and W_λ require $d^2 \log(n)$ polylog($d, 1/\epsilon$) qubits to implement gates R_i , see Fig. 5.
- (4) Overall, the total number of auxiliary qubits needed is $d^2 \log(n)$ polylog($d, 1/\epsilon$).

The above analysis finishes the proof of the second statement of Theorem 1.1.

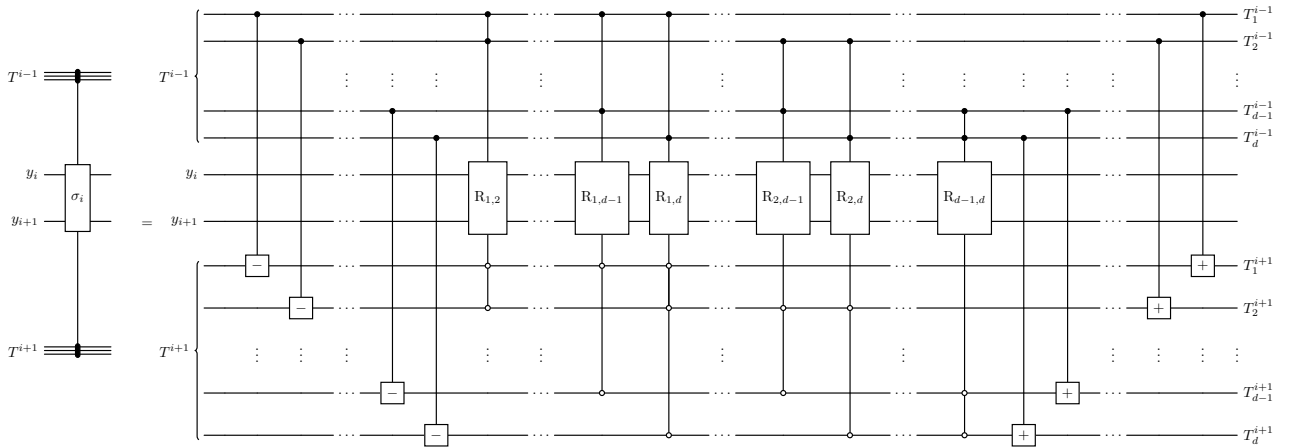


FIGURE 11. Quantum circuit implementing the transposition σ_i in the Yamanouchi encoding is similar to the circuit in the standard encoding, see Fig. 4. Controlled “ \pm ” gates and rotation $R_{j,k}$ gates are exactly the same as on Fig. 4.

5. QUANTUM CIRCUITS FOR OPTIMIZED RESOURCE STATES

In this section, we describe efficient quantum circuits for preparing optimized resource states for the aforementioned PBT protocols. To write and present such circuits in a unified way, we shall introduce another

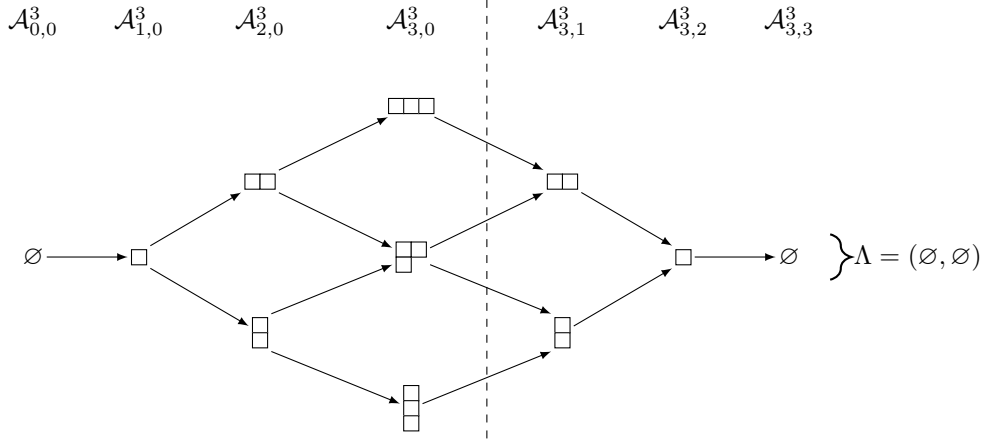


FIGURE 12. A part of Bratteli diagram $\hat{\mathcal{B}}$ corresponding to an irrep $\Lambda = (\emptyset, \emptyset)$ of algebra $\mathcal{A}_{3,3}^3$. The set of paths starting at the root and terminating at the end span the Gelfand–Tsetlin basis of $\Lambda = (\emptyset, \emptyset)$. A tensor product of n copies of EPR states shared between the first and second half of the systems is fully supported in irrep $\Lambda = (\emptyset, \emptyset)$ in the Schur basis. In fact, it corresponds to a uniform superposition of all symmetric paths in the Gelfand–Tsetlin basis, see eqs. (83) and (84). Similarly, the optimized resource state for PBT protocols can be expressed as a weighted superposition of symmetric paths in the Gelfand–Tsetlin basis. In particular, for pPBT the exact formula for the weights might be computed in $\tilde{O}(d)$ time, see eq. (91), while for dPBT, weights are the result of non-trivial optimization procedure, see eq. (92).

variant of mixed Schur transform $U_{\text{Sch}}(n, n)$ corresponding to the matrix algebra $\mathcal{A}_{n,n}^d$ of partially transposed permutations acting on $n + n$ qudits, each of local dimension d . Note that this short introduction is analogous, yet not identical, to the one presented in Sections 2.2 and 2.3. Again, we refer the more interested reader to [GBO23] for more details.

The matrix algebra $\mathcal{A}_{n,n}^d$ is generated by acting on $(\mathbb{C}^d)^{\otimes n+n}$ in a similar way as (6). Its irreducible representations are labelled by the following pairs of Young diagrams:

$$\hat{\mathcal{A}}_{n,n}^d := \left\{ (\lambda, \mu) \mid \lambda \vdash n - k, \mu \vdash n - k, \ell(\lambda) + \ell(\mu) \leq d, \text{ for } k \in [n] \right\}. \quad (78)$$

Furthermore, we adapt the Okounkov–Vershik approach to describe representation theory of $\hat{\mathcal{A}}_{n,n}^d$, together with the notion of the Bratteli diagram $\hat{\mathcal{B}}$ for the sequence of algebras $\mathcal{A}_{0,0}^d \hookrightarrow \mathcal{A}_{1,0}^d \hookrightarrow \dots \hookrightarrow \mathcal{A}_{n,0}^d \hookrightarrow \mathcal{A}_{n,1}^d \hookrightarrow \dots \hookrightarrow \mathcal{A}_{n,n}^d$, and the notion of paths in the Bratteli diagram $\text{Paths}(\Lambda, \hat{\mathcal{B}})$ starting at the root and terminating at Λ . As we shall see, for our purpose it is enough to present only one special representation corresponding to irrep $\Lambda = (\emptyset, \emptyset) \in \hat{\mathcal{A}}_{n,n}^d$. The set of paths

$$\text{Paths}((\emptyset, \emptyset), \hat{\mathcal{B}}) := \left\{ (T^0, \dots, T^n, T^{n+1}, \dots, T^{2n}) \mid T^k, T^{2n-k} \vdash k \text{ for } k \leq n, \text{ and} \right. \quad (79)$$

$$\left. T^{i-1} \rightarrow T^i, T^{2n-i+1} \rightarrow T^{2n-i} \text{ for } i \in [n] \right\} \quad (80)$$

span the Gelfand–Tsetlin basis $\{|T\rangle \mid T \in \text{Paths}(\Lambda, \hat{\mathcal{B}})\}$ of irreducible representation $(\emptyset, \emptyset) \in \hat{\mathcal{A}}_{n,n}^d$, see Fig. 12. Furthermore, for $\mu \vdash k$, $k \leq n$, we denote by $\text{Paths}_n(\mu, \hat{\mathcal{B}})$ the set of all paths which terminate in μ at the level k . Notice that for $i \in [n]$ the diagram T^i is obtained from T^{i-1} by adding some addable cell $a \in \text{AC}_d(T^{i-1})$, while for $i > n$ the diagram T^i is obtained from T^{i-1} by removing some cell.

A variant of mixed Schur–Weyl duality partitions the space $(\mathbb{C}^d)^{\otimes n+n}$ into subspaces that are invariant under the natural $U^{\otimes n} \otimes \bar{U}^{\otimes n}$ action of $U \in U_d$ and the action of the matrix algebra $\mathcal{A}_{n,n}^d$. It implies existence of mixed quantum Schur transform $U_{\text{Sch}}(n, n) \in U_{d^{n+n}}$, a unitary basis change $U_{\text{Sch}}(n, n) \in U_{d^{n+n}}$ that maps the computational basis $\{|x\rangle \mid x \in [d]^{n+n}\}$ of $(\mathbb{C}^d)^{\otimes n+n}$ to a new basis composed of irreducible representations \mathcal{W}_Λ and \mathcal{H}_Λ of the aforementioned actions of U_d and $\mathcal{A}_{n,n}^d$, respectively:

$$U_{\text{Sch}}(n, n): (\mathbb{C}^d)^{\otimes n+n} \rightarrow \bigoplus_{\Lambda \in \hat{\mathcal{A}}_{n,n}^d} \mathcal{H}_\Lambda \otimes \mathcal{W}_\Lambda \quad \text{where } \mathcal{H}_\Lambda := \mathbb{C}^{\text{Paths}(\Lambda, \hat{\mathcal{B}})} \text{ and } \mathcal{W}_\Lambda := \mathbb{C}^{\text{GT}(\Lambda)}, \quad (81)$$

where the direct sum ranges over all irreducible representations Λ of $\mathcal{A}_{n,n}^d$, and $\text{GT}(\Lambda)$ denotes the set of, so-called, Gelfand–Tsetlin patterns, see [GBO23] for more details. Similarly as in Section 2.2, transformation (81)

extends to the following isometry

$$U_{\text{Sch}}(n, n): (\mathbb{C}^d)^{\otimes n+1} \rightarrow \underbrace{\mathbb{C}^{\hat{\mathcal{A}}_{0,0}^d} \otimes \dots \otimes \mathbb{C}^{\hat{\mathcal{A}}_{n,n}^d}}_T \otimes \underbrace{\mathbb{C}^{\text{GT}((n,n),d)}}_{M_{[d-1]}}, \quad (82)$$

where paths $T \in \text{Paths}(\hat{\mathcal{B}})$ is stored as a tensor product state $|T\rangle = |T^2\rangle \otimes \dots \otimes |T^{n+n}\rangle$. In [GBO23], we described a quantum circuit implementing the mixed Schur isometry, which for any computational basis vector outputs the corresponding superposition of paths $T \in \text{Paths}(\hat{\mathcal{B}})$ and Gelfand–Tsetlin patterns. The complexity of implementing the mixed quantum Schur transform isometry $U_{\text{Sch}}(n, n)$ is $\tilde{O}(nd^4)$ [Ngu23; GBO23].

A tensor product of n copies of EPR states shared between the first and second half of the systems in $(\mathbb{C}^d)^{\otimes n+n}$ has a relatively simple form in mixed Schur basis [SSMH17]. In particular, it is supported only on one irrep, namely $\Lambda = (\emptyset, \emptyset) \in \hat{\mathcal{A}}_{n,n}^d$. Notice that the unitary group representation corresponding to $\Lambda = (\emptyset, \emptyset)$ is one dimensional. With a small abuse of notation, we have

$$U_{\text{Sch}}(n, n) \left(\bigotimes_{i=1}^n |\Phi^+\rangle_{A_i B_i} \right) = \sum_{\mu \vdash_d n} \sqrt{\frac{d_\mu m_\mu}{d^n}} |\text{EPR}_\mu^{[n-1]}\rangle |\mu\rangle_{T^n}, \quad (83)$$

where

$$|\text{EPR}_\mu^{[n-1]}\rangle := \sum_{S \in \text{Paths}_n(\mu, \hat{\mathcal{B}})} \sqrt{\frac{1}{d_\mu}} |S_0\rangle_{T^0} \dots |S_{n-1}\rangle_{T^{n-1}} |S_{n-1}\rangle_{T^{n+1}} \dots |S_0\rangle_{T^{2n}} \quad (84)$$

and $|\Phi^+\rangle_{A_i B_i} := \frac{1}{\sqrt{d}} \sum_{k=1}^d |k\rangle_{A_i} |k\rangle_{B_i}$ is an EPR pair shared between Alice's register i and Bob's register i . Notice that the order of the path registers is slightly changed compared to (82), and all paths present in the formula above are symmetric with respect to the middle vertex. The analytical expressions for optimized resource states in dPBT and pPBT protocols were developed in Ref [SSMH17; MSSH18; Chr+21], and in a mixed Schur basis have a similar form to n copies of EPR pairs (83). Indeed, in both cases, they are of the following form

$$|\Psi\rangle_T = \sum_{\mu \vdash_d n} \sqrt{f_\mu} |\text{EPR}_\mu^{[n-1]}\rangle |\mu\rangle_{T^n}, \quad (85)$$

where $\{f_\mu\}_{\mu \vdash_d n}$ is some probability distribution satisfying $\sum_{\mu \vdash_d n} f_\mu = 1$.⁷ Furthermore, we can rewrite this expression as

$$|\Psi\rangle_T = \sum_{\lambda \vdash_d n-1} \sqrt{f_\lambda} |\text{EPR}_\lambda^{[n-2]}\rangle |\lambda\rangle_{T^{n-1}} |\lambda\rangle_{T^{n+1}} \left(\sum_{a \in \text{AC}_d(\lambda)} \sqrt{\frac{f_{\lambda \cup a} d_\lambda}{f_\lambda d_{\lambda \cup a}}} |\lambda \cup a\rangle_{T^n} \right), \quad (86)$$

$$|\text{EPR}_\lambda^{[n-2]}\rangle := \sum_{S \in \text{Paths}_{n-1}(\lambda, \hat{\mathcal{B}})} \sqrt{\frac{1}{d_\lambda}} |S_0\rangle_{T^0} \dots |S_{n-2}\rangle_{T^{n-2}} |S_{n-2}\rangle_{T^{n+2}} \dots |S_0\rangle_{T^{2n}}, \quad (87)$$

where f_λ are defined in such a way that the state $\sum_{a \in \text{AC}_d(\lambda)} \sqrt{\frac{f_{\lambda \cup a} d_\lambda}{f_\lambda d_{\lambda \cup a}}} |\lambda \cup a\rangle_{T^n}$ is normalized, namely

$$\frac{f_\lambda}{d_\lambda} := \sum_{a \in \text{AC}_d(\lambda)} \frac{f_{\lambda \cup a}}{d_{\lambda \cup a}}. \quad (88)$$

We continue doing this rewriting recursively. That leads to the circuit for the preparation of $|\Psi\rangle_T$ presented in Fig. 13, where gates F_i prepare the following states controlled on T^{i-1} :

$$F_i |\nu\rangle_{T^{i-1}} |0\rangle_{T^i} = |\nu\rangle_{T^{i-1}} \left(\sum_{a \in \text{AC}_d(\nu)} \sqrt{\frac{f_{\nu \cup a} d_\nu}{f_\nu d_{\nu \cup a}}} |\nu \cup a\rangle_{T^i} \right) \quad (89)$$

In particular, for pPBT [SSMH17] the formulas for f_ν for every $\nu \vdash_d k$ turn out to be as follows:

$$f_\nu = \frac{m_\nu^2}{\sum_{\chi \vdash_d k} m_\chi^2} \quad (90)$$

Therefore due to [SSMH17, Proposition 25] and eq. (47) the amplitudes in eq. (89) for every $a \in \text{AC}_d(\nu)$ and $\nu \vdash k$ can be computed efficiently in time $\tilde{O}(d)$:

$$\frac{f_{\nu \cup a} d_\nu}{f_\nu d_{\nu \cup a}} = \frac{d + \text{cont}(a) m_{\nu \cup a}}{d^2 + k} \frac{m_{\nu \cup a}}{m_\nu} = \frac{d + \text{cont}(a)}{d^2 + k} \left(\prod_{\substack{i: i \neq r \\ 1 \leq i \leq d}} \frac{\nu_r - \nu_i + i - r + 1}{\nu_r - \nu_i + i - r} \right), \quad (91)$$

⁷In PBT literature sometimes a different parametrization used: $f_\mu = \frac{c_\mu d_\mu m_\mu}{d^n}$ where c_μ are variables. EPR resource state corresponds to the choice $c_\mu = 1$ for every $\mu \vdash_d n$.

where the last equality is due to the Weyl dimension formula eq. (14) and r denotes the row number where the box a was added to Young diagram ν .

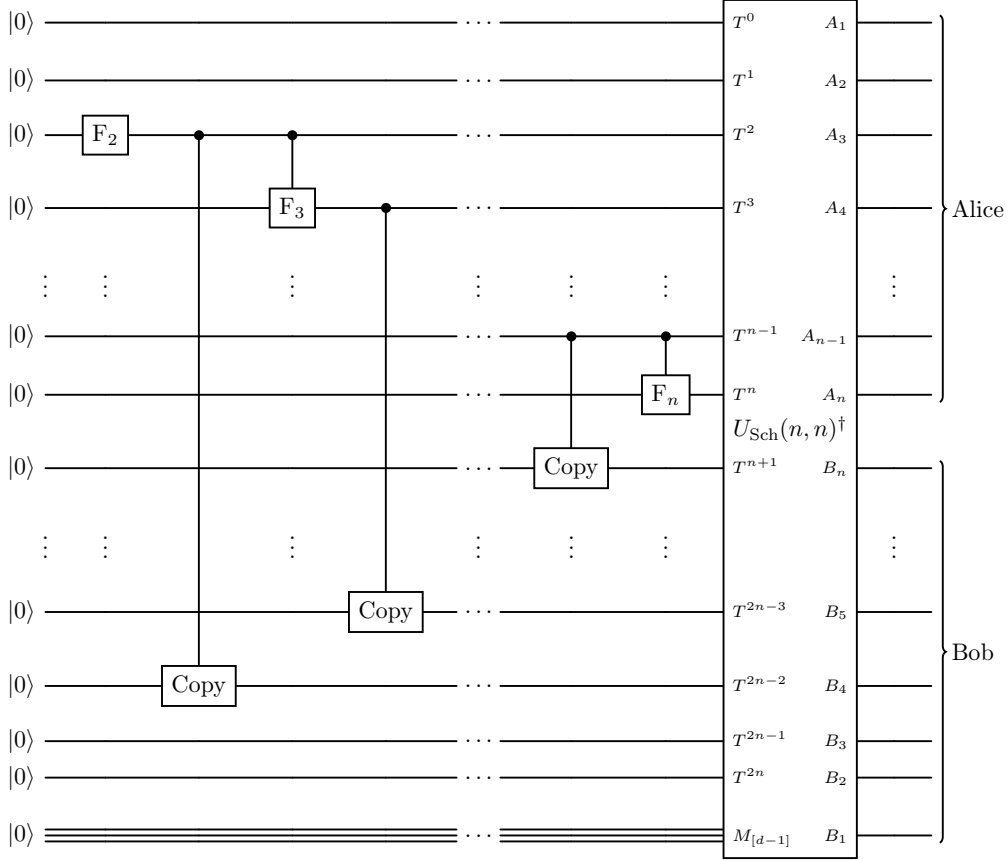


FIGURE 13. Circuit for the preparation of the resource state $|\Psi\rangle_T|0\rangle_{M_{[d-1]}}$ from eq. (85). Gates F_i are defined in eq. (89) via eqs. (90) and (91).

However, we cannot do the same analysis for the dPBT protocol [MSSH18; Led20] since f_μ for $\mu \vdash_d n$ are defined via non-trivial optimization problem [Led20, Equation 6.3]:

$$\{f_\mu\}_{\mu \vdash_d n} = \arg \max_{\sum_\mu f_\mu = 1} \sum_{\lambda \vdash_d n-1} \left(\sum_{a \in \text{AC}_d(\lambda)} \sqrt{f_{\lambda \cup a}} \right)^2. \quad (92)$$

We leave it as an open question for future work to understand how to efficiently compute the amplitudes in eq. (89) for dPBT. At the same time, a suboptimal choice for dPBT resource states, described in [Chr+21, Section B], are implementable via our scheme presented above.

ACKNOWLEDGEMENTS

DG thanks Tudor Giurgica-Tiron, Quynh Nguyen, Aram Harrow, Hari Krovi, Yanlin Chen and John van de Wetering for useful general discussions. We thank Adam Wills for his comments about known results on port-based teleportation, for pointing out logarithmic space Schur transform from [WS23], and for useful general discussions. We also thank Rene Allerstorfer, Harry Burhman, Florian Speelman and Philip Verduyn Lunel for discussing the relationship between port-based teleportation and non-local quantum computation. Finally, we thank all authors of [Ngu23; FTH23] for the coordination with version 1 of [GBO23] which initially described the efficient dPBT construction, now presented in the current paper. DG, AB, and MO were supported by an NWO Vidi grant (Project No VI.Vidi.192.109).

REFERENCES

- [ABMSL23] Rene Allerstorfer, Harry Burhman, Alex May, Florian Speelman, and Philip Verduyn Lunel. “Relating non-local quantum computation to information theoretic cryptography”. In: (2023). arXiv: [2306.16462](#) [quant-ph] (cit. on p. 2).
- [ABSL22] Rene Allerstorfer, Harry Burhman, Florian Speelman, and Philip Verduyn Lunel. “On the Role of Quantum Communication and Loss in Attacks on Quantum Position Verification”. In: (2022). arXiv: [2208.04341](#) [quant-ph] (cit. on p. 2).

- [Ben+93] Charles H Bennett, Gilles Brassard, Claude Crépeau, Richard Jozsa, Asher Peres, and William K Wootters. “Teleporting an unknown quantum state via dual classical and Einstein-Podolsky-Rosen channels”. In: *Physical review letters* 70.13 (1993), p. 1895 (cit. on p. 1).
- [BK11] Salman Beigi and Robert König. “Simplified instantaneous non-local quantum computation with applications to position-based cryptography”. In: *New Journal of Physics* 13.9 (2011), p. 093036 (cit. on pp. 2, 16).
- [Buh+16] Harry Buhrman, Łukasz Czekaj, Andrzej Grudka, Michał Horodecki, Paweł Horodecki, Marcin Markiewicz, Florian Speelman, and Sergii Strelchuk. “Quantum communication complexity advantage implies violation of a Bell inequality”. In: *Proceedings of the National Academy of Sciences* 113.12 (2016), pp. 3191–3196 (cit. on p. 2).
- [Chr+21] Matthias Christandl, Felix Leditzky, Christian Majenz, Graeme Smith, Florian Speelman, and Michael Walter. “Asymptotic performance of port-based teleportation”. In: *Communications in Mathematical Physics* 381.1 (2021), pp. 379–451. DOI: [10.1007/s00220-020-03884-0](https://doi.org/10.1007/s00220-020-03884-0). arXiv: [1809.10751](https://arxiv.org/abs/1809.10751) (cit. on pp. 2, 8, 20, 21).
- [DJR04] Thomas Decker, Dominik Janzing, and Martin Rötteler. “Implementation of group-covariant positive operator valued measures by orthogonal measurements”. In: *Journal of Mathematical Physics* 46.1 (Dec. 2004). DOI: [10.1063/1.1827924](https://doi.org/10.1063/1.1827924). arXiv: [quant-ph/0407054](https://arxiv.org/abs/quant-ph/0407054). URL: <http://dx.doi.org/10.1063/1.1827924> (cit. on p. 7).
- [FTH23] Jiani Fei, Sydney Timmerman, and Patrick Hayden. “Efficient Quantum Algorithm for Port-based Teleportation”. In: (2023). arXiv: [2310.01637](https://arxiv.org/abs/2310.01637) [[quant-ph](https://arxiv.org/abs/2310.01637)] (cit. on pp. 3, 21).
- [GBO23] Dmitry Grinko, Adam Burchardt, and Maris Ozols. “Gelfand–Tsetlin basis for partially transposed permutations and mixed quantum Schur transform”. In: (2023). arXiv: [2310.02252](https://arxiv.org/abs/2310.02252) [[quant-ph](https://arxiv.org/abs/2310.02252)] (cit. on pp. 3–7, 10, 12, 13, 15–17, 19–21).
- [GBW21] Martina Gschwendtner, Andreas Bluhm, and Andreas Winter. “Programmability of covariant quantum channels”. In: *Quantum* 5 (June 2021), p. 488. DOI: [10.22331/q-2021-06-29-488](https://doi.org/10.22331/q-2021-06-29-488). arXiv: [2012.00717](https://arxiv.org/abs/2012.00717) (cit. on p. 2).
- [GO22] Dmitry Grinko and Maris Ozols. “Linear programming with unitary-equivariant constraints”. In: (2022). arXiv: [2207.05713](https://arxiv.org/abs/2207.05713) (cit. on pp. 2–5).
- [HW94] Paul Hausladen and William K. Wootters. “A ‘pretty good’ measurement for distinguishing quantum states”. In: *Journal of Modern Optics* 41.12 (1994), pp. 2385–2390. DOI: [10.1080/09500349414552221](https://doi.org/10.1080/09500349414552221) (cit. on p. 7).
- [IH08] Satoshi Ishizaka and Tohya Hiroshima. “Asymptotic teleportation scheme as a universal programmable quantum processor”. In: *Phys. Rev. Lett.* 101.24 (Dec. 2008), p. 240501. DOI: [10.1103/PhysRevLett.101.240501](https://doi.org/10.1103/PhysRevLett.101.240501). arXiv: [0807.4568](https://arxiv.org/abs/0807.4568) (cit. on pp. 1, 2).
- [IH09] Satoshi Ishizaka and Tohya Hiroshima. “Quantum teleportation scheme by selecting one of multiple output ports”. In: *Physical Review A* 79.4 (2009), p. 042306 (cit. on pp. 1, 2).
- [Ish15] Satoshi Ishizaka. *Some remarks on port-based teleportation*. 2015. arXiv: [1506.01555](https://arxiv.org/abs/1506.01555) [[quant-ph](https://arxiv.org/abs/1506.01555)] (cit. on p. 2).
- [KMSH21] Piotr Kopszak, Marek Mozrzyk, Michał Studziński, and Michał Horodecki. “Multiport based teleportation – transmission of a large amount of quantum information”. In: *Quantum* 5 (Nov. 2021), p. 576. DOI: [10.22331/q-2021-11-11-576](https://doi.org/10.22331/q-2021-11-11-576). arXiv: [2008.00856](https://arxiv.org/abs/2008.00856) (cit. on p. 2).
- [Kos03] Masashi Kosuda. “A new proof for some relations among axial distances and hook-lengths”. In: *Tokyo Journal of Mathematics* 26.1 (2003), pp. 199–228 (cit. on p. 12).
- [KS18] William M. Kirby and Frederick W. Strauch. “A practical quantum algorithm for the Schur transform”. In: *Quantum Information & Computation* 18.9&10 (2018), pp. 721–742. DOI: [10.26421/QIC18.9-10-1](https://doi.org/10.26421/QIC18.9-10-1). arXiv: [1709.07119](https://arxiv.org/abs/1709.07119) (cit. on p. 3).
- [Led20] Felix Leditzky. “Optimality of the pretty good measurement for port-based teleportation”. 2020. arXiv: [2008.11194](https://arxiv.org/abs/2008.11194) (cit. on pp. 2, 7, 21).
- [Lou08] James D. Louck. *Unitary Symmetry and Combinatorics*. World Scientific Publishing Company, 2008. URL: <https://books.google.com/books?id=akZkDQAAQBAJ> (cit. on p. 5).
- [May19] Alex May. “Quantum tasks in holography”. In: *Journal of High Energy Physics* 2019.10 (2019), pp. 1–39 (cit. on pp. 2, 16).
- [May22] Alex May. “Complexity and entanglement in non-local computation and holography”. In: *Quantum* 6 (2022), p. 864 (cit. on pp. 2, 16).
- [MSK21] Marek Mozrzyk, Michał Studziński, and Piotr Kopszak. “Optimal multi-port-based teleportation schemes”. In: *Quantum* 5 (June 2021), p. 477. DOI: [10.22331/q-2021-06-17-477](https://doi.org/10.22331/q-2021-06-17-477). arXiv: [2011.09256](https://arxiv.org/abs/2011.09256) (cit. on p. 2).
- [MSSH18] Marek Mozrzyk, Michał Studziński, Sergii Strelchuk, and Michał Horodecki. “Optimal port-based teleportation”. In: *New Journal of Physics* 20.5 (May 2018), p. 053006. DOI: [10.1088/1367-2630/aab8e7](https://doi.org/10.1088/1367-2630/aab8e7). arXiv: [1707.08456](https://arxiv.org/abs/1707.08456) (cit. on pp. 2, 7, 8, 20, 21).
- [NC97] Michael A. Nielsen and Isaac L. Chuang. “Programmable quantum gate arrays”. In: *Physical Review Letters* 79.2 (July 1997), pp. 321–324. DOI: [10.1103/PhysRevLett.79.321](https://doi.org/10.1103/PhysRevLett.79.321). arXiv: [quant-ph/9703032](https://arxiv.org/abs/quant-ph/9703032) (cit. on p. 2).
- [Ngu23] Quynh T. Nguyen. “The mixed Schur transform: efficient quantum circuit and applications”. In: (2023). arXiv: [2310.01613](https://arxiv.org/abs/2310.01613) [[quant-ph](https://arxiv.org/abs/2310.01613)] (cit. on pp. 3, 5, 6, 13, 20, 21).
- [PBP21] Jason Pereira, Leonardo Banchi, and Stefano Pirandola. “Characterising port-based teleportation as universal simulator of qubit channels”. In: *Journal of Physics A: Mathematical and Theoretical* 54.20 (2021), p. 205301 (cit. on p. 2).

- [PLLP19] Stefano Pirandola, Riccardo Laurenza, Cosmo Lupo, and Jason L Pereira. “Fundamental limits to quantum channel discrimination”. In: *npj Quantum Information* 5.1 (2019), p. 50 (cit. on p. 2).
- [Sag13] Bruce E. Sagan. *The symmetric group: representations, combinatorial algorithms, and symmetric functions*. Graduate Texts in Mathematics. Springer New York, 2013. URL: <https://books.google.com/books?id=Y6vTBwAAQBAJ&pg> (cit. on p. 10).
- [SMK22] Michał Studziński, Marek Mozrzyk, and Piotr Kopszak. “Square-root measurements and degradation of the resource state in port-based teleportation scheme”. In: *Journal of Physics A: Mathematical and Theoretical* 55.37 (2022), p. 375302 (cit. on p. 2).
- [SMKH22] Michał Studziński, Marek Mozrzyk, Piotr Kopszak, and Michał Horodecki. “Efficient multi port-based teleportation schemes”. In: *IEEE Transactions on Information Theory* (2022). DOI: [10.1109/TIT.2022.3187852](https://doi.org/10.1109/TIT.2022.3187852). arXiv: [2008.00984](https://arxiv.org/abs/2008.00984) (cit. on p. 2).
- [Spe16] Florian Speelman. “Instantaneous non-local computation of low T -depth quantum circuits”. In: *11th Conference on the Theory of Quantum Computation, Communication and Cryptography (TQC 2016)*. Ed. by Anne Broadbent. Vol. 61. Leibniz International Proceedings in Informatics (LIPIcs). Dagstuhl, Germany: Schloss Dagstuhl–Leibniz-Zentrum fuer Informatik, 2016, 9:1–9:24. DOI: [10.4230/LIPIcs.TQC.2016.9](https://doi.org/10.4230/LIPIcs.TQC.2016.9) (cit. on p. 16).
- [SS23] Sergii Strelchuk and Michał Studziński. “Minimal port-based teleportation”. In: *New Journal of Physics* (2023) (cit. on pp. 2, 7, 8).
- [SSMH17] Michał Studziński, Sergii Strelchuk, Marek Mozrzyk, and Michał Horodecki. “Port-based teleportation in arbitrary dimension”. In: *Scientific reports* 7.1 (Sept. 2017), p. 10871. DOI: [10.1038/s41598-017-10051-4](https://doi.org/10.1038/s41598-017-10051-4). arXiv: [1612.09260](https://arxiv.org/abs/1612.09260) (cit. on pp. 2, 7, 8, 20).
- [Sta13] Richard Stanley. “Algebraic combinatorics”. In: *Springer* 20.22 (2013), p. 4 (cit. on p. 10).
- [Ste87] John R Stembridge. “Rational tableaux and the tensor algebra of \mathfrak{gl}_n ”. In: *Journal of Combinatorial Theory, Series A* 46.1 (1987), pp. 79–120 (cit. on p. 4).
- [WHS23] Adam Wills, Min-Hsiu Hsieh, and Sergii Strelchuk. “Efficient Algorithms for All Port-Based Teleportation Protocols”. In: (2023). arXiv: [2311.12012](https://arxiv.org/abs/2311.12012) [quant-ph] (cit. on p. 3).
- [WS23] Adam Wills and Sergii Strelchuk. “Generalised Coupling and An Elementary Algorithm for the Quantum Schur Transform”. In: (2023). arXiv: [2305.04069](https://arxiv.org/abs/2305.04069) [quant-ph] (cit. on pp. 3, 21).
- [YRC20] Yuxiang Yang, Renato Renner, and Giulio Chiribella. “Optimal Universal Programming of Unitary Gates”. In: *Phys. Rev. Lett.* 125 (21 Nov. 2020), p. 210501. DOI: [10.1103/PhysRevLett.125.210501](https://doi.org/10.1103/PhysRevLett.125.210501). arXiv: [2007.10363](https://arxiv.org/abs/2007.10363) (cit. on p. 2).